Cronfa
Swansea University's Research Repository

Meson Masses in the Unquenched Quark Model

Jack Kennelly

Submitted to Swansea University in fulfilment of the requirements for the Degree of MSc
Swansea University
2022

Copyright: The author, Jack Kennelly, 2022.

Abstract

A novel approach to calculating coupled-channel effects for bottomonium in the $^3P_0$ framework using realistic wavefunctions is introduced in which the physical state is expanded in a basis set of harmonic oscillators. Other techniques of solving the unquenched system are also presented including perturbative, simple harmonic oscillator and unique valence approximations. The resulting (spin-averaged) mass shifts are calculated for an $nS \to 1S+1S$ transition and compared across the separate methods. It is determined that the largest effect on the mass shift across the various approaches is the accurate treatment of the wavefunction, which causes significant deviations from the simple harmonic oscillator approximation near threshold. It is also found that the inclusion of mixing between valence states due to meson loops has no effect at ground state energies but induces small differences at higher lying states. While conclusions are drawn about the relative effect each of the methods presented have on determining the mass shift due to unquenching, further research is suggested for other transitions to be assured in such conclusions.

Declarations and Statements

This work has not previously been accepted in substance for any degree and is not being concurrently submitted in candidature for any degree.

Signed: Jack Kennelly
Date: 13/04/2022

This thesis is the result of my own investigations, except where otherwise stated. Other sources are acknowledged by explicit references. A bibliography is appended.

Signed: Jack Kennelly
Date: 13/04/2022

I hereby give consent for my thesis, if accepted, to be available for photocopying and for inter-library loan, and for the title and summary to be made available to outside organisations.

Signed: Jack Kennelly
Date: 13/04/2022

The university's ethical procedures have been followed and, where appropriate, that ethical approval has been granted.

Signed: Jack Kennelly
Date: 13/04/2022

Contents

Acknowledgements

The author is grateful to Dr. Timothy Burns for providing excellent discussions, material and insights into the subject matter of the thesis and wider physics field, without whom this work would not be realised.

List of Tables

List of Figures

1 Introduction

Quantum Chromodynamics (QCD) establishes the gauge field theory of strong interactions, which are responsible for binding quarks into hadrons, in the SU(3) component of the standard model [4]. There are many different techniques that have been developed to perform calculations within the QCD framework that each have their merits and limitations. One approach is perturbative QCD which can be effective in the high energy region and at short distances because the strong coupling constant is small in these limits and thus the expansion in perturbation theory converges, thereby producing a valid approximation to the system. However, while asymptotic freedom is a perturbative concept that is useful in describing these restricted areas of the field, low energy behaviour (such as confinement) or processes dependent on large-distance contributions can make the expansion parameter large and therefore pQCD becomes unsuitable for these types of calculations [5, 6]. In these sectors, lattice QCD provides a non-perturbative approach whereby the characteristics of QCD are implemented onto a discretised Euclidean space-time grid and unlike pQCD, can be used in problems involving confinement and has a well behaved renormalisation factors as the lattice spacing approaches zero, among other features [7]. With that being said, the methods used within this framework such as monte carlo simulations can be extremely computationally intensive, so much so that lattice QCD systems are often studied in the context of exploring techniques to improve numerical efficiency, for example applications of mixed precision solvers on GPUs [8] and even machine learning [9].

To avoid the large calculation work associated with LQCD, one can use quark models to 'reproduce the behaviour of observables such as the spectrum and magnetic moments in the baryon and meson sector' [10]. The first quark models were developed in the 1960s by works from Greenberg [11] and

Dalitz [12] in which the harmonic oscillator model of Baryons was formulated. The harmonic oscillator, along with the Hydrogen atom, is one of the few confining potentials for which the Schrödinger equation can be solved analytically, but since these works many other potentials have been studied such as the Morse, Pösch-Teller, complex cube, anhormonic oscillator and quarkonium potentials, the most common of which however is the coulomb plus linear, or Cornell, potential. Furthermore, a plethora of analytical and numerical techniques have been implemented into finding approximate solutions to these potentials including, but not limited to, super-symmetric quantum mechanics, the WKB method, Nikiforov Uvarov's method and the asymptotic iteration method (AIM) [13]. However, quenched quark models neglect non-valence quark effects such as meson creation and continuum coupling mechanisms in their formalism or absorb these phenomena into the model parameters [14]. Because of this, and despite the fact that there has been some successes using screened potentials to account for such effects [15], efforts have been made in unquenching the quark model to treat these mechanisms, and the resulting mass shifts induced by meson loops, more fundamentally. To do this, various models have been formulated to calculate the $q\bar{q}$ light mesons in the continuum. One such framework, which will be assumed in this paper, is the $^3\mathrm{P}_0$ model in which the light meson pair is created out of the vacuum thereby sharing the associated 0^{++} quantum numbers causing it to be in a spin triplet state [16]. The $^3\mathrm{P}_0$ operator has been used extensively in unquenched quark models for a variety of hadronic states including Charmonia, Bottomonia, charmed mesons, bottom mesons and baryons [17]. Other models include the flux tube model in which the $q\bar{q}$ pair are formed via a breaking of the gluonic flux tube between the quarks (which in Isgur and Paton's work [18, 19] is derived from the strong coupling expansion of Lattice QCD) and also microscopic models wherein 'pair creation arises from the same interaction which controls the hadronic spectrum, so that masses and decays are determined by the same parameters' [17].

Whilst the potential models are approximate by nature and may not appreciate some of the underlying physics as much as more complicated formalisms like lattice QCD, techniques by which to account for hadronic loop effects are nonetheless important. Previously, it was thought they could be responsible for the anomalously low masses of some charm-strange states and such mechanisms are only partially present in quenched lattice QCD [2]. More recently, this form of QCD is less justifiable as it neglects these aspects of the calculation, whilst modern research in this area include diagrams that allow for hadron loop effects [20]. It is therefore reasonable to argue that undertaking research to make quark models more accurate is a worthwhile endeavour that could provoke some significant results, and such improvements are not limited to the inclusion of hadronic loop corrections.

Whilst there has been extensive research in unquenched or 'coupled-channel' effects, particularly within the $^3P_0$ model, most of these calculations involve a simple harmonic oscillator approximation to the wavefunction to simplify the problem without clear clarification on it's validity [1]. The work presented in this thesis aims to not only introduce a novel approach to solving the unquenched system for bottomonium that uses more realistic wavefunctions, but also to provide a comprehensive comparison to three other methods that produce such solutions under various frameworks and approximations. This novel approach involves a matrix system of solving the Schrödinger equation in which the real, orthonormal wavefunction is expanded in a basis set of harmonic oscillators and both the discrete and continuum sectors of the problem are solved simultaneously. Within this comparison is a perturbative approach to the problem and one that is solved self consistently within the coupled-channel equations that both adhere to the aforementioned single SHO wavefunctions. Also included is a technique that uses the harmonic oscillator expansion for the wavefunction, but under the single valence approximation such that there is no sum over the discrete eigenstates. By performing the same calculation with identical parameters using four sepa-

rate methods, conclusions will be drawn regarding the relative effect each set of techniques and approximations has on the induced mass shift due to meson loops. This thesis will be organised as follows. Section 2 will derive the methods discussed from first principles which leads onto section 3 in which the theory is contextualised to mesons. The potential model and solution to the discrete spectrum is discussed in section 4, followed by the computation of the necessary matrix elements in section 5. Data and results are analysed in section 6 and are presented alongside those in [1] for comparative purposes, while conclusions and final thoughts are summarised in section 7.

2 Theory

2.1 Nomenclature

In the following derivations, the notation is chosen to be general in form such as to not disrupt the flow of the logic with unnecessary detail at this stage. $|n\rangle$ describes the initial state of the heavy meson, whilst $|\lambda p\rangle$ represents the heavy-light mesons in the continuum. Here, p denotes their relative momentum whilst the remaining relevant information, such as radial, spin, orbital and angular momentum quantum numbers, as well as flavour, are absorbed into the object λ. $|\psi\rangle$ represents the physical state, which is itself an admixture of discrete and continuum states.

2.2 The Hamiltonian

The Hamiltonian for the unquenched system will be expressed as

$$H = H_0 + U \tag{1}$$

where H_0 is the part of the Hamiltonian that just acts on one part of the wavefunction, the bare state $|n\rangle$ or the continuum state $|\lambda p\rangle$:

$$H_0 |n\rangle = M_n |n\rangle \tag{2}$$

$$H_0 |\lambda p\rangle = E_\lambda(p) |\lambda p\rangle . \tag{3}$$

with M_n denoting the mass of the state $|n\rangle$ and $E_\lambda(p)$ the energy of the continuum mesons, dependent on their relative momentum p. The following equations define the orthogonality relations between both the discrete and

continuum components of the wavefunction

$$\langle n'|n\rangle = \delta_{n'n}, \tag{4}$$

$$\langle \lambda' p'|\lambda p\rangle = \frac{\delta_{\lambda'\lambda}\delta\left(p'-p\right)}{p^2}, \tag{5}$$

$$\langle \lambda p|n\rangle = 0. \tag{6}$$

The term U couples the discrete and continuum sectors via $\langle \lambda p|U|n\rangle$. This is the matrix element that is responsible for coupling the bare meson $(Q\bar{q})$ to the two meson state $(Q\bar{q})(\bar{Q}q)$. This term, however, does not contribute to coupling between the valence states

$$\langle m|U|n\rangle = 0 \tag{7}$$

and conversely, H_0 does not contribute to mixing between discrete and continuum states

$$\langle \lambda p|H_0|n\rangle = 0. \tag{8}$$

The Hamiltonian, H, used in this thesis has no spin dependence due to the approximations discussed in Section 3.2 and therefore the results obtained correspond to spin-averaged masses, which can be determined using the equation

$$M = \frac{1}{4}\left(3\Upsilon + \eta_b\right). \tag{9}$$

2.3 Wavefunction and Normalisation

The time-independent Schrödinger equation is

$$H\left|\psi\right\rangle = E\left|\psi\right\rangle \tag{10}$$

where $|\psi\rangle$ is the real orthonormal wavefunction. Since H mixes $|n\rangle$ and $|\lambda p\rangle$, the wavefunction is an admixture of both components, in the form

$$|\psi\rangle = \sum_n |n\rangle \langle n|\psi\rangle + \sum_\lambda \int dp\ p^2 |\lambda p\rangle \langle \lambda p|\psi\rangle . \tag{11}$$

The normalisation condition necessitates:

$$\langle \psi|\psi\rangle = 1, \tag{12}$$

hence

$$\sum_m |\langle m|\psi\rangle|^2 + \sum_\lambda \int dp\ p^2 |\langle \lambda p|\psi\rangle|^2 = 1 \tag{13}$$

which follows from the orthogonality relations (4), (5) and (6). In some cases the single valence approximation is applied, where the wavefunction constitutes only one discrete state and a range of continuum states. Thus, there is a simpler form of (11) with no sum over the valence states.

$$|\psi\rangle = |n\rangle \langle n|\psi\rangle + \sum_\lambda \int dp\ p^2 |\langle \lambda p|\psi\rangle|^2 \tag{14}$$

with normalisation

$$|\langle n|\psi\rangle|^2 + \sum_\lambda \int dp\ p^2 |\langle \lambda p|\psi\rangle|^2 = 1 \tag{15}$$

2.4 The Mass Shift Equation

The inclusion of coupled-channel effects, responsible for the transition of a heavy meson $(Q\bar{Q})$ into two heavy-light mesons $((Q\bar{q}), (\bar{Q}q))$, causes a change in the mass of the state. As various methods for solving the unquenched system are derived, the object $\Omega(W)$ is used to obtain the mass shift and

mixing matrix in each case, and is defined by

$$\Omega(W) = \sum_{\lambda} \int dp\ p^2\ \frac{U\,|\lambda p\rangle\,\langle \lambda p|\,U}{E_\lambda(p) - W}. \tag{16}$$

The argument W is an object that will be defined on a case by case basis as different methods of deriving this relation are discussed.

2.5 Perturbation Theory

The method outlined in this section is based in perturbation theory by assuming the term U in the Hamiltonian, that is responsible for mixing the valence and continuum states, is a small effect in comparison to H_0 in determining the masses and properties of the states, and can therefore be modelled as a perturbation to the system. In this setup, the Hamiltonian takes the form

$$H = H_0 + aU \tag{17}$$

where H_0 is the spectrum of base states and a is the book keeping parameter used to track powers in the expansion. The full eigenstates, $|\psi\rangle$, are solutions of (10). Performing a power series expansion:

$$\begin{aligned} |\psi\rangle &= |n\rangle + a\,|\phi^{(1)}\rangle + a^2\,|\phi^{(2)}\rangle + \dots \\ E &= M_n + aE^{(1)} + a^2E^{(2)} + \dots . \end{aligned} \tag{18}$$

This can then be substituted into (10), and since this must be true for any a, the coefficients can be equated. The $\mathcal{O}\,(a^0)$ result is just the defining equation of the base states (2). However, powers of a give the following equations:

$\mathcal{O}\,(a)$:

$$H_0\,|\phi^{(1)}\rangle + U\,|n\rangle = M_n\,|\phi^{(1)}\rangle + E^{(1)}\,|n\rangle \tag{19}$$

$\mathcal{O}(a^2)$:

$$H_o |\phi^{(2)}\rangle + U |\phi^{(1)}\rangle = M_n |\phi^{(2)}\rangle + E_n^{(1)} |\phi^{(1)}\rangle + E_n^{(2)} |n\rangle \tag{20}$$

First Order

Multiplying (19) on the left with $\langle n|$ gives

$$\langle n| H_0 |\phi^{(1)}\rangle + \langle n| U |n\rangle = M_n \langle n|\phi^{(1)}\rangle + E^{(1)}. \tag{21}$$

Then, using the relations (2) and (7) this becomes

$$M_n \langle n|\phi^{(1)}\rangle + 0 = M_n \langle n|\phi^{(1)}\rangle + E^{(1)} \tag{22}$$

and so the first order contribution to the energy is zero. Now, multiplying (19) on the left with $\langle \lambda p|$ and using equations (2) and (6) gives the expression

$$E_\lambda(p) \langle \lambda p|\phi^{(1)}\rangle + \langle \lambda p| U |n\rangle = M_n \langle \lambda p|\phi^{(1)}\rangle + 0 \tag{23}$$

which when simplified forms the equation:

$$\langle \lambda p|\phi^{(1)}\rangle = \frac{\langle \lambda p| U |n\rangle}{M_n - E_\lambda(p)}. \tag{24}$$

This is the continuum component of the first order correction to the wave-function. As for the discrete component, rearranging (19) and multiplying on the left with $\langle m|$ gives

$$\langle m| H_0 - M_n |\phi^{(1)}\rangle = \langle m| E^{(1)} - U |n\rangle . \tag{25}$$

Since the first order correction to the energy is zero, and using (2), this can be expressed as

$$(M_m - M_n) \langle m|\phi^{(1)}\rangle = 0. \tag{26}$$

Equation (26) implies that, for $m \neq n$, $\langle m|\phi^{(1)}\rangle = 0$, i.e. to first order there is no mixing between different valence states. On the other hand, if $m = n$, equation (26) does not have any constraint on $\langle n|\phi^{(1)}\rangle$. This can also be seen by noting that, given a solution $|\phi^{(1)}\rangle$ to equation (19), the linear combination $|\phi^{(1)}\rangle\, c\, |n\rangle$ is also a solution, for arbitrary c. This freedom in the definition of the first order wavefunction is a generic feature of non-degenerate perturbation theory, as discussed in [21]. The usual approach is followed of insisting the first order correction to the wavefunction is orthogonal to the zeroth order wavefunction, in that $\langle n|\phi^{(1)}\rangle = 0$. As happens in the case of ordinary first order perturbation theory, other definitions are possible and these unfold differently at the point of normalising the wavefunction, which is beyond the scope of this thesis. Using equations (11) and (24),

$$|\phi^{(1)}\rangle = \sum_{\lambda} \int dp\, |\lambda p\rangle\, \frac{\langle \lambda p|\, U\, |n\rangle}{M_n - E_\lambda(p)}. \tag{27}$$

Second Order

From (20),

$$(H_0 - M_n)\, |\phi^{(2)}\rangle - E^{(2)}\, |n\rangle = (E^{(1)} - U)\, |\phi^{(1)}\rangle\,. \tag{28}$$

Using (11), and the fact that $E^{(1)} = 0$, gives

$$(H_0 - M_n)\, |\phi^{(2)}\rangle - E^{(2)}\, |n\rangle = -\sum_{\lambda} \int dp\; p^2\; U\, |\lambda p\rangle\, \langle \lambda p|\phi^{(1)}\rangle\,. \tag{29}$$

Multiplying on the left with $\langle m|$ and simplifying produces the relation

$$(M_m - M_n)\, \langle m|\phi^{(2)}\rangle - E^{(2)}\, \langle m|n\rangle = -\sum_{\lambda} \int dp\; p^2\, \langle m|U|\lambda p\rangle\, \langle \lambda p|\phi^{(1)}\rangle\,. \tag{30}$$

If $m = n$,

$$\begin{aligned} E^{(2)} &= \sum_{\lambda} \int dp\ p^2 \langle n|U|\lambda p\rangle \langle \lambda p|\phi^{(1)}\rangle \\ &= \sum_{\lambda} \int dp\ p^2 \frac{|\langle \lambda p|U|n\rangle|^2}{M_n - E_\lambda(p)} \end{aligned} \tag{31}$$

by virtue of (24). If $m \neq n$, then due to (4), the equation becomes

$$\langle m|\phi^{(2)}\rangle = \frac{1}{M_n - M_m} \sum_{\lambda} \int dp\ p^2 \frac{\langle m|U|\lambda p\rangle \langle \lambda p|U|n\rangle}{M_n - E_\lambda(p)}, \tag{32}$$

and thus, using (11):

$$|\phi^{(2)}\rangle = \sum_{m} |m\rangle \frac{1}{M_n - M_m} \sum_{\lambda} \int dp\ p^2 \frac{\langle m|U|\lambda p\rangle \langle \lambda p|U|n\rangle}{M_n - E_\lambda(p)}. \tag{33}$$

In summary, the correction to the energy to second order is

$$E = M_n + \sum_{\lambda} \int dp\ p^2 \frac{|\langle \lambda p|U|n\rangle|^2}{M_n - E_\lambda(p)}. \tag{34}$$

Since the context of this framework is below threshold, $M_n < E_\lambda(p)$ for all p and thus E is real. Equation (16) then becomes

$$M_n - E = \langle n|\Omega(M_n)|n\rangle = \sum_{\lambda} \int dp\ p^2 \frac{\langle n|\, U\, |\lambda p\rangle \langle \lambda p|\, U\, |n\rangle}{E_\lambda(p) - M_n} \tag{35}$$

where $\langle n|\Omega(M_n)|n\rangle$ is the mass shift. While this appears to be a transcendental equation, M_n can be calculated using the methods outlined in section 4 and thus can be inserted into (35) to find E. This setup corresponds to Case 1 in the results and discussion.

2.6 Single Valence Approximation

In this approach, the problem is solved self consistently by varying E to find a solution whilst using the single valence approximation such that there is no sum over discrete states, i.e. look for solutions to (10) of the form

$$E\,|\psi\rangle = H\,|n\rangle\,\langle n|\psi\rangle + \sum_{\lambda}\int dp\; p^2 H\,|\lambda p\rangle\,\langle \lambda p|\psi\rangle\,. \tag{36}$$

As before, multiplying on the left with $\langle n|$, and using (2) and (8) to simplify, produces the relation

$$(E - M_n)\,\langle n|\psi\rangle = \sum_{\lambda}\int dp\; p^2\,\langle n|U|\lambda p\rangle\,\langle \lambda p|\psi\rangle\,. \tag{37}$$

Now, multiplying (36) on the left with $\langle \lambda' p'|$ and using (8) gives

$$E\,\langle \lambda' p'|\psi\rangle = \langle \lambda' p'|U|n\rangle\,\langle n|\psi\rangle + E_\lambda(p)\,\langle \lambda' p'|\psi\rangle \tag{38}$$

which can be simplified using (5) and re-arranging:

$$(E - E_\lambda(p))\,\langle \lambda p|\psi\rangle = \langle \lambda p|U|n\rangle\,\langle n|\psi\rangle\,. \tag{39}$$

Substituting the above into (37) gives the familiar mass shift equation (16)

$$M_n - E = \langle n|\Omega(E)|n\rangle = \sum_{\lambda}\int dp\; p^2 \frac{|\langle \lambda p|U|n\rangle|^2}{E_\lambda(p) - E} \tag{40}$$

except now with argument E instead of the discrete mass M_n. Since E is unknown at this point, (40) becomes a transcendental equation and is therefore somewhat difficult to solve, requiring a graphical or numerical approach, which will be detailed in due course. This method is represented by Case 2 in following sections of the thesis.

2.7 Treating the Discrete Wavefunction

In the previous two approaches, the wavefunction at the point of coupling between the valence and continuum states, i.e. in $\langle n|\Omega(W)|n\rangle$, is assumed to be a single simple harmonic oscillator as is often done in the literature [2]. Thus, writing $|N\rangle$ as a harmonic oscillator state,

$$\langle n|\Omega(W)|n\rangle \rightarrow \langle N|\Omega(W)|N\rangle \tag{41}$$

in Cases 1 and 2. However, one can treat the discrete wavefunction as an eigenstate of H_0 at this point, as in equation (2), via an expansion in the harmonic oscillator basis:

$$|n\rangle = \sum_N |N\rangle \langle N|n\rangle \,. \tag{42}$$

Since perturbation theory is inherently approximate anyway, this treatment of the wavefunction is more appropriately applied to the 'coupled-channel' setup and so from equation (40)

$$\langle n|\Omega(E)|n\rangle = \sum_{N'N} \langle n|N'\rangle \langle N'|\Omega(W)|N\rangle \langle N|n\rangle \,. \tag{43}$$

This forms a matrix equation

$$\begin{aligned} &M_n - E = \\ &\begin{pmatrix} \langle n|1\rangle & \langle n|2\rangle & \dots \end{pmatrix} \begin{pmatrix} \langle 1|\Omega(E)|1\rangle & \langle 1|\Omega(E)|2\rangle & \dots \\ \langle 2|\Omega(E)|1\rangle & \langle 2|\Omega(E)|2\rangle & \dots \\ \vdots & \vdots & \ddots \end{pmatrix} \begin{pmatrix} \langle 1|n\rangle \\ \langle 2|n\rangle \\ \vdots \end{pmatrix} \end{aligned} \tag{44}$$

where the eigenvectors of H_0 are dot multiplied with the full $\Omega(E)$ matrix. This method of applying the single valence approximation using realistic wavefunctions will be referred to as Case 3.

2.8 Summing Over Discrete Eigenstates

In contrast to the previous sections, the following technique for solving the problem discusses a general case in which the single valence approximation is not assumed. Thus, solutions of (10) are searched for in the form

$$E\,|\psi\rangle = \sum_n H\,|n\rangle\,\langle n|\psi\rangle + \sum_\lambda \int dp\; p^2 H\,|\lambda p\rangle\,\langle \lambda p|\psi\rangle\,. \tag{45}$$

Multiplying the above on the left with $\langle m|$ and using (4), (2) and (8) to simplify gives

$$\begin{aligned} E\,\langle m|\psi\rangle &= \sum_n \delta_{mn} M_n\,\langle n|\psi\rangle + \sum_\lambda \int dp\; p^2\,\langle m|U|\lambda p\rangle\,\langle \lambda p|\psi\rangle \\ &= M_m\,\langle m|\psi\rangle + \sum_\lambda \int dp\; p^2\,\langle m|U|\lambda p\rangle\,\langle \lambda p|\psi\rangle\,. \end{aligned} \tag{46}$$

Hence, with $m \to n$:

$$(E - M_n)\,\langle n|\psi\rangle = \sum_\lambda \int dp\; p^2\,\langle n|U|\lambda p\rangle\,\langle \lambda p|\psi\rangle\,. \tag{47}$$

Multiplying (45) on the left with $\langle \lambda' p'|$ and using (4), (5) and (8) to simplify produces the relation

$$\begin{aligned} E\,\langle \lambda' p'|\psi\rangle &= \sum_n \langle \lambda' p'|U|n\rangle\,\langle n|\psi\rangle \\ &\quad + \sum_\lambda \int dp\; p^2 E_\lambda(p) \frac{\delta_{\lambda'\lambda}\delta(p'-p)}{p^2}\,\langle \lambda p|\psi\rangle\,, \\ &= \sum_n \langle \lambda' p'|U|n\rangle\,\langle n|\psi\rangle + E_{\lambda'}(p')\,\langle \lambda' p'|\psi\rangle\,. \end{aligned} \tag{48}$$

Hence,

$$(E - E_\lambda(p)) \langle \lambda p|\psi\rangle = \sum_n \langle \lambda p|U|n\rangle \langle n|\psi\rangle \,. \tag{49}$$

Substituting this into (47) gives

$$\begin{aligned}(E - M_n) \langle n|\psi\rangle &= \sum_\lambda \int dp\; p^2 \frac{\langle n|U|\lambda p\rangle}{E - E_\lambda(p)} \times \sum_m \langle \lambda p|U|m\rangle \langle m|\psi\rangle \\ &= \sum_m \Omega_{mn}(E) \langle m|\psi\rangle\end{aligned} \tag{50}$$

with

$$\Omega_{mn}(E) = \sum_\lambda \int dp\; p^2 \frac{\langle n|U|\lambda p\rangle \langle \lambda p|U|m\rangle}{E - E_\lambda(p)}. \tag{51}$$

This can also be written as

$$\sum_m (\delta_{mn} M_m + \Omega_{mn}(E)) \langle m|\psi\rangle = E \langle n|\psi\rangle \tag{52}$$

which is a matrix equation

$$\begin{aligned}&\left[\begin{pmatrix} M_1 & 0 & \dots \\ 0 & M_2 & \dots \\ \vdots & \vdots & \ddots \end{pmatrix} + \begin{pmatrix} \Omega_{11}(E) & \Omega_{12}(E) & \dots \\ \Omega_{21}(E) & \Omega_{22}(E) & \dots \\ \vdots & \vdots & \ddots \end{pmatrix} \right] \begin{pmatrix} \langle 1|\psi\rangle \\ \langle 2|\psi\rangle \\ \vdots \end{pmatrix} = \\ &E \begin{pmatrix} \langle 1|\psi\rangle \\ \langle 2|\psi\rangle \\ \vdots \end{pmatrix}\end{aligned} \tag{53}$$

or, more simply

$$\left(\underline{\underline{M}} + \underline{\underline{\Omega}}(E)\right) \underline{\Phi} = E\underline{\Phi}. \tag{54}$$

The eigenvalues are found by solving

$$\left|\underline{\underline{M}} + \underline{\underline{\Omega}}(E) - E\underline{\underline{I}}\right| = 0. \tag{55}$$

The practical difficulty with this method is that it requires the discrete wavefunctions to be obtained numerically which is cumbersome to implement as an input into the matrix, especially at large dimensions. Consequently, one typically uses harmonic oscillator wavefunctions as an approximation to make the computation viable, particularly when considering a wide range of states and transitions. This is a limiting feature of this approach that is related to the separation of discrete and mixing components of the calculation, thus the following technique is suggested.

2.9 Valence Mixing

The procedure by which the mass shift is derived in this case is a novel approach to the problem that takes advantage of the full set of harmonic oscillator basis states by allowing a self-contained treatment of the discrete and unquenching parts simultaneously, without the need to compromise on the discrete component of the wavefunction at the point of coupling with the continuum. As before, the wavefunction is defined using the completeness relation (11), except now the harmonic oscillator state $|N\rangle$ is used as opposed to a discrete eigenstate of H_0. Thus, instead of having (2), which implies the relation

$$\langle m|H_0|n\rangle = M_n\delta_{mn}, \tag{56}$$

the equation becomes

$$\langle N'|H_0|N\rangle = \begin{pmatrix} \langle 1|H_0|1\rangle & \langle 1|H_0|2\rangle & \dots \\ \langle 2|H_0|1\rangle & \langle 2|H_0|2\rangle & \dots \\ \vdots & \vdots & \ddots \end{pmatrix}. \tag{57}$$

From here, the same process is followed with solutions found for (10) in the form of (45). Multiplying on the left with $\langle N'|$ gives

$$E\,\langle N'|\psi\rangle = \sum_N \langle N'|H_0|N\rangle\,\langle N'|\psi\rangle + \sum_\lambda \int dp\; p^2\,\langle N'|U|\lambda p\rangle\,\langle \lambda p|\psi\rangle\,. \tag{58}$$

Multiplying on the left with $\langle \lambda' p'|$ gives

$$E\,\langle \lambda' p'|\psi\rangle = \sum_N \langle \lambda' p'|U|N\rangle\,\langle N|\psi\rangle + \sum_\lambda \int dp\; p^2\,\langle \lambda' p'|H_o|\lambda p\rangle\,\langle \lambda p|\psi\rangle \tag{59}$$

which, using (5) and (3) and removing primes, reduces to

$$(E - E_\lambda(p))\,\langle \lambda p|\psi\rangle = \sum_N \langle \lambda p|U|N\rangle\,\langle N|\psi\rangle\,. \tag{60}$$

Substituting this into (58) produces the equation

$$\begin{aligned} E\,\langle N'|\psi\rangle &= \sum_N \langle N'|H_0|N\rangle\,\langle N|\psi\rangle + \sum_{N\lambda} \int dp\; p^2 \frac{\langle N'|U|\lambda p\rangle\,\langle \lambda p|U|N\rangle}{E - E_\lambda(p)}\,\langle N|\psi\rangle \\ &= \sum_N \left(\langle N'|H_0|N\rangle + \langle N'|\Omega(E)|N\rangle\right)\langle N|\psi\rangle \end{aligned} \tag{61}$$

where $\Omega(E)$ is identical to that of (51). Defining

$$\mathcal{H}(E) = H_0 + \Omega(E) \tag{62}$$

means the system of equations can be expressed as

$$\sum_N \langle N'|\mathcal{H}(E)|N\rangle \langle N|\psi\rangle = E \langle N'|\psi\rangle \tag{63}$$

which is a matrix equation

$$\begin{pmatrix} \langle 1|\mathcal{H}(E)|1\rangle & \langle 1|\mathcal{H}(E)|2\rangle & \dots \\ \langle 2|\mathcal{H}(E)|1\rangle & \langle 2|\mathcal{H}(E)|2\rangle & \dots \\ \vdots & \vdots & \ddots \end{pmatrix} \begin{pmatrix} \langle 1|\psi\rangle \\ \langle 2|\psi\rangle \\ \vdots \end{pmatrix} = E \begin{pmatrix} \langle 1|\psi\rangle \\ \langle 2|\psi\rangle \\ \vdots \end{pmatrix}, \tag{64}$$

or

$$\underline{\underline{\mathcal{H}}}(E)\underline{\Phi} = E\underline{\Phi}, \tag{65}$$

with solutions found by solving

$$\left|\underline{\underline{\mathcal{H}}}(E) - E\underline{\underline{I}}\right| = 0. \tag{66}$$

The benefit of this setup is not only that it allows the full problem to be solved concurrently, making computation much simpler, but it also allows mixing between the different valence states by not conceding the discrete aspect of the wavefunction to simple harmonic oscillator forms. This mixing arises from the unquenching where coupling between the various valence states is due to meson loops. This method will be referred to as Case 4 in the sections to follow.

In summary, Case 1 is a perturbative approach to the problem by using a power series expansion to find solutions to (10). Case 2 involves using the single valence approximation such that the system is described by one discrete state and a range of continuum states, and the resulting transcendental equation is solved by varying E to find a solution. Case 3 is also derived and solved in this manner, except the discrete wavefunction is also expanded in a basis set of harmonic oscillators to better approximate the true wavefunc-

tion. As described, case 4 is a novel approach that does not assume a single valence model and allows mixing between various discrete states whilst also allowing both aspects of the problem to be solved simultaneously.

3 Contextualisation

3.1 Mesons in this Framework

At this stage, it is necessary to map the previous notation to the context of mesons, and in doing so, classify both aspects of the problem using the appropriate quantum numbers and approximations. Previously, $|n\rangle$ was used to describe the bare $(Q\bar{Q})$ state whilst $|\lambda p\rangle$ was used to describe the heavy-light mesons in the continuum $((Q\bar{q}),(q\bar{Q}))$. Now, the relevant quantum numbers will be added to this nomenclature in the following way:

$$\begin{aligned} |n\rangle &\rightarrow |nSLJ\rangle \\ |\lambda p\rangle &\rightarrow |n_1 S_1 L_1 J_1, n_2 S_2 L_2 J_2, jl, f, p\rangle \end{aligned} \tag{67}$$

where n,S,L and J denote the usual radial, spin, orbital and angular momentum quantum numbers respectively. Furthermore,

$$\underline{J_1} + \underline{J_2} = \underline{j} \tag{68}$$

and l is the relative orbital angular momentum of mesons 1 and 2 in the continuum. To conserve angular momentum,

$$\underline{j} + \underline{l} = \underline{J}. \tag{69}$$

Moreover, in order to conserve parity, l is constrained by

$$(-)^l = (-)^{L+L_1+L_2+1}. \tag{70}$$

3.2 Simplifying the Model

In principle, one should sum over all possible continuum states in equation (67), but since the largest contributions to $\Omega(E)$ come from the continuua with the smallest masses, due to the energy denominator in (16), the model can be simplified. This can be done by restricting the continuum mesons to radial ground states ($n_1 = n_2 = 0$) and S-wave states ($L_1 = L_2 = 0$). Since

$$\underline{S_i} + \underline{L_i} = \underline{J_i} \tag{71}$$

it follows that

$$\underline{S_i} = \underline{J_i} \tag{72}$$

and thus keeping both $\underline{S_i}$ and $\underline{J_i}$ quantum numbers becomes unnecessary, so $\underline{J_i}$ is discarded. Now,

$$|\lambda p\rangle \rightarrow |S_1 S_2, jl, f, p\rangle \tag{73}$$

and so equation (16), with the appropriate bra and ket vectors applied, becomes

$$\begin{aligned} &\langle \hat{n}\hat{S}\hat{L}J|\Omega(E)|nSLJ\rangle \\ &= \sum_{S_1 S_2 jlf} \int_0^\infty dp\ p^2 \frac{\langle \hat{n}\hat{S}\hat{L}J|U|S_1 S_2 jlfp\rangle \langle S_1 S_2 jlfp|U|nSLJ\rangle}{E - E_{S_1 S_2 f}(p)} \end{aligned} \tag{74}$$

with

$$E_{S_1 S_2 f}(p) = \sqrt{m_{S_1 f}^2 + p^2} + \sqrt{m_{S_2 f}^2 + p^2} \tag{75}$$

and angular momentum J conserved in the interaction.

3.2.1 Angular Momentum Coefficients and Spatial Factors

At this point, it is useful to utilize some other works in this field in order to further simplify the problem. The results presented in [17] show that the matrix element pertaining to the unquenching aspect of the problem factorises into three terms: a quark flavour factor, a coefficient dependent upon the quark spin degrees of freedom of the mesons and a term relating to their spatial wavefunctions. This allows the numerator in (74) to be expressed as

$$\langle S_1 S_2 jlfp|U|nSLJ\rangle = C_f \xi_{jl}(SLJ \to S_1 S_2)\mathcal{M}_l(nL) \tag{76}$$

where C_f, ξ_{jl} and $\mathcal{M}_l(nL)$ are the flavour, angular momentum and spatial factors respectively. The angular momentum factor is simply a coefficient which can be directly taken from tables in [17], whilst the spatial factors are explicitly given in the appendix of [2] for each $^3\mathrm{P}_0$ transition amplitude and will be specified later. Using these properties allows the calculation to become more straightforward since the flavour and angular momentum terms can be taken outside the integral to avoid direct computation. Not only does this simplify the solution to such integrals, but reduces computation time which is very beneficial in numerical calculations.

3.2.2 Mass Splitting and Spin

Now, due to the above, (74) takes the form

$$\begin{aligned}\langle \hat{n}\hat{S}\hat{L}J|\Omega(E)|nSLJ\rangle = &\sum_{S_1 S_2 jl} \xi_{jl}(\hat{S}\hat{L}J \to S_1 S_2)\xi_{jl}(SLJ \to S_1 S_2) \\ &\times \sum_f C_f^2 \int_0^\infty dp\ p^2 \frac{\mathcal{M}_l(\hat{n}\hat{L})\mathcal{M}_l(nL)}{E - E_{S_1 S_2 f}(p)}.\end{aligned} \tag{77}$$

However, the calculation can become simpler still if the mass splitting between continuum states of a given flavour are ignored, ie

$$\begin{aligned} M_{B*} &= M_B \\ M_{Bs*} &= M_{B_s} \end{aligned} \tag{78}$$

where M_B and M_{B_s} denote the masses of the associated B mesons in the continuum. The continuum masses and energies are therefore independent of S_1 and S_2, i.e.

$$m_{S_1 f} = m_{S_2 f} \equiv m_f \tag{79}$$

and

$$E_{S_1 S_2 f} \equiv E_f. \tag{80}$$

As a result, the integral no longer depends upon S_1 or S_2 and because of this, the orthogonality property of the angular momentum terms, which ultimately derives from the orthogonality of Clebsch-Gordan coefficients, can be utilized [17]:

$$\sum_{S_1 S_2 j} \xi_{jl}(\hat{S}\hat{L}J \to S_1 S_2)\xi_{jl}(SLJ \to S_1 S_2) = \delta_{\hat{S}S}\delta_{\hat{L}L} \tag{81}$$

which would not have been possible if the integral had spin dependence. Equation (74) therefore becomes

$$\langle \hat{n}\hat{S}\hat{L}J|\Omega(E)|nSLJ\rangle = \delta_{\hat{S}S}\delta_{\hat{L}L}\sum_f C_f^2 \sum_l \int_0^\infty dp\ p^2 \frac{\mathcal{M}_l(\hat{n}\hat{L})\mathcal{M}_l(nL)}{E - E_f(p)}. \tag{82}$$

Moreover, if H_0 is also taken to be spin-independent then

$$\langle \hat{n}\hat{S}\hat{L}J|H_0|nSLJ\rangle = \delta_{\hat{S}S}\delta_{\hat{L}L}\langle \hat{n}L|H_0|nL\rangle . \tag{83}$$

Since there are $\delta_{\hat{S}S}$ and $\delta_{\hat{L}L}$ functions in both the discrete and continuum terms, there is no mixing between states with different spin or orbital angular momentum, which means when constructing basis sets, S and L are fixed and

are thus good quantum numbers.

Now, the relevant expressions for the calculation have no dependence on S or J and so these quantum numbers can be ignored, simply constructing bases $|nL\rangle$. Equation (82) therefore becomes

$$\langle \hat{n}L|\Omega(E)|nL\rangle = \sum_f C_f^2 \sum_l \int_0^\infty dp\ p^2\ \frac{\mathcal{M}_l(\hat{n}L)\mathcal{M}_l(nL)}{E - E_f(p)}. \tag{84}$$

Since the equations are now independent of S and J, the solutions, or eigenstates, will also be independent of S and J and thus states that only share the same L will be degenerate.

3.2.3 Justification of Approximations

In order to perform the aforementioned approximations to the model, it is necessary to provide the appropriate line of reasoning in order to ensure their usage does not detract from the use of the model itself, especially when the approximations are not consistent with experimental data.

Firstly, it has been shown in relevant literature that the unquenching effects that cause these mass shifts being studied are approximately spin independent, in that states within a given L set with different S and J quantum numbers are affected in the same way [22]. Furthermore, residual spin dependent effects can be understood using [17] without it being imperative to perform the full calculation for all S and J. Secondly, this work is primarily focused on the overall effects on a given L multiplet as opposed to the differences within it as this is already understood. In essence, unquenching effects reduce the spin splittings such that the splittings in the physical state are suppressed with respect to those in the valence state by a spin-averaged valence component [23] and thus it becomes unnecessary to repeatedly perform

the calculation for all S and J. Lastly, while they are in no way essential to the method of calculation, the approximations put forth in this section do make the calculation significantly simpler to perform. This may not be a justification per se, but it is nonetheless a worthwhile endeavour, especially if one were needed to perform the calculation numerous times for different transitions and decays.

Now that the methods by which to solve the unquenched system have been presented and the necessary approximations made, the discrete part of the problem pertaining to the initial heavy meson $(Q\bar{Q})$ state can be solved. A solution for the matrix element in 84 will then be found and the mass shift due to the $(Q\bar{Q}) \to (Q\bar{q})(\bar{Q}q)$ loop can be determined.

4 Potential Model and Discrete Spectrum

4.1 Cornell Potential Model

At this stage, it is necessary to solve the Hamiltonian of the bare state and therefore specify the potential model used for this aspect of the calculation. Since this section is concerned with solving the Schrödinger equation in the quenched limit, there is no coupling term U in the Hamiltonian, which for the non-relativistic potential model is defined as

$$H = T + V(r) + V_{sd}(r) + 2m_q + c \tag{85}$$

where c denotes the mass renormalization factor. In this model, the Cornell potential will be used which has the form

$$V(r) = -\frac{4}{3}\frac{b}{r} + \sigma r \tag{86}$$

with b representing the strength of colour Coulomb potential and σ the strength of linear confinement. Also in the Hamiltonian is the spin dependent term $V_{sd}(r)$ which determines the mass splitting within the multiplets. However, as stated in the previous section, this work is focused on the overall effects on a given L multiplet as opposed to the mass splitting within it and therefore this term will be ignored for the main body of the thesis. Nevertheless, one can account for this by treating it as a perturbation to the system in a similar fashion to the coupling term in Case 1. A derivation of this is included in the appendix.

4.2 Model Parameters

$m_b = 4.5\text{GeV}$	$m_u = m_d = 0.33\text{GeV}$	$m_s = 0.5\text{GeV}$
$b = 0.34$	$\sigma = 0.22\text{GeV}^2$	$c = 0.435\text{GeV}^2$
	$\gamma = 0.205$	

Table 1: The parameters used in the calculations to produce the bare mass M_n and mass shift $-\Delta M$ as shown in table 2, taken from [1] for comparative purposes. These were chosen in such a way to 'reproduce the dielectric decay widths of $\Upsilon(nS), n = 1, 2, 3$' wherein a comparison was made to [2] and data from the Particle Data Group (PDG) [3]

Table 1 contains the relevant masses of bottomonium, m_b, and the constituent quarks $m_u = m_d$ and m_s for the up/down and strange variations respectively. It also includes values for parameters in the Cornell potential model and the dimensionless coupling constant, represented by γ. This parameter selection was taken from [1] so that the methods and corresponding data presented in this thesis can be compared such that any differences can be analysed knowing it did not arise due to the choice of potential model parameters.

4.3 Expansion in Harmonic Oscillator Basis

In order to solve the Schrödinger equation for this Hamiltonian, the real, orthonormal wavefunctions are expanded in the harmonic oscillator set of basis functions.

$$\Psi_{nlm}(r, \theta, \phi) = \sum_{NLM} C^{nlm}_{NLM} \Phi_{NLM}(r, \theta, \phi) \tag{87}$$

Since $V(r)$ is a central potential, in that it depends on the magnitude of r but not the vector, l is a good quantum number as states are not mixtures of different orbital angular momentum. Using the reduced mass, the potential

of the harmonic oscillator is

$$V_{ho}(r) = \frac{4\alpha^4}{m_b} r^2 \tag{88}$$

where α controls the width of the potential. The harmonic oscillator wavefunctions are expressed as

$$\Phi_{NLM}(r,\theta,\phi) = \sqrt{\frac{N! \times 2^{L+\frac{5}{2}} \alpha^{2L+3}}{\left(N+L+\frac{1}{2}\right)!}} r^L e^{-\alpha^2 r^2} L_N^{L+\frac{1}{2}} \left(2\alpha^2 r^2\right) Y_L^M(\theta,\phi) \tag{89}$$

with $L_N^{L+\frac{1}{2}}\left(2\alpha^2 r^2\right)$ representing an associated Laguerre Polynomial and $Y_L^M(\theta,\phi)$ the usual spherical harmonic [21]. In general, the associated Laguerre polynomial is defined as [24]

$$L_n^k(x) = \sum_{m=0}^{n} (-1)^m \frac{(n+k)!}{(n-m)!(k+m)!m!} x^m \tag{90}$$

With the first few polynomials given by

$$L_0^k(x) = 1 \tag{91}$$

$$L_1^k(x) = -x + k + 1 \tag{92}$$

$$L_2^k(x) = \frac{1}{2}\left(x^2 - 2\left(k+2\right)x + \left(k+1\right)\left(k+2\right)\right). \tag{93}$$

Multiplying equation (87) by the conjugate harmonic oscillator wavefunction and integrating produces delta functions on the right hand side pertaining to the quantum numbers N,L and M due to the orthogonality principle. This gives rise to the relation

$$C_{NLM}^{nlm} = \int \Phi_{NLM}^*(\underline{r}) \Psi_{nlm}(\underline{r}) d^3\underline{r}. \tag{94}$$

The spherical harmonics contained within the wavefunctions above are also orthogonal and as such, can be reduced to delta functions when being integrated:

$$C_{NLM}^{nlm} = \delta_{Ll}\delta_{Mm}\int_0^\infty R_{NL}(r)R_{nl}(r)r^2dr. \tag{95}$$

Substituting this into equation (87) gives

$$\Psi_{nlm}(r,\theta,\phi) = \sum_N C_N^{nl}\Phi_{NLM}(r,\theta,\phi) \tag{96}$$

which produces the following radial Schrödinger equation after cancelling the associated spherical harmonics

$$\sum_N C_N^{nl}\hat{H}R_{Nl}(r) = E^{nl}R_{nl}(r). \tag{97}$$

Multiplying this by the primed radial wavefunction and integrating produces the relation

$$\begin{aligned}\sum_N C_N^{nl}\int_0^\infty R_{N'l}(r)\hat{H}R_{Nl}(r)r^2dr &= E^{nl}\int_0^\infty R_{N'l}R_{nl}(r)r^2dr \\ &= E^{nl}C_{N'}^{nl}\end{aligned} \tag{98}$$

creating a matrix equation

$$\begin{pmatrix} H_{11} & H_{12} & \cdots \\ H_{21} & H_{22} & \cdots \\ \vdots & \vdots & \ddots \end{pmatrix}\begin{pmatrix} C_1^{nl} \\ C_2^{nl} \\ \vdots \end{pmatrix} = E^{nl}\begin{pmatrix} C_1^{nl} \\ C_2^{nl} \\ \vdots \end{pmatrix}. \tag{99}$$

by denoting $H_{N'N}$ as $\int_0^\infty R_{N'l}(r)\hat{H}R_{Nl}(r)r^2dr$. To solve this, one simply constructs the $H_{N'N}$ matrix and finds the associated eigenvalues E^{nl} and corresponding eigenvectors, but first a method of calculating the matrix element $H_{N'N}$, or $\langle N'l|H|Nl\rangle$, is required. The Hamiltonian of the harmonic

oscillator is

$$H_{ho} = T + V_{ho}(r) \tag{100}$$

which can be rearranged to account for the kinetic term T, thus (85) can be replaced with

$$H = H_{ho} - V_{ho}(r) + V(r) + 2m_q + c. \tag{101}$$

This is a useful substitution because the eigenvalues of H_{ho} are known and therefore using the Schrödinger equation, and the fact that the associated wavefunctions are orthonormal, $\langle N'l|H_{ho}|Nl\rangle$ can be evaluated:

$$\langle N'l|H_{ho}|Nl\rangle = \frac{2\alpha^2}{m_b}\left(2N + l + \frac{3}{2}\right)\delta_{N'N}. \tag{102}$$

By introducing the change of variables $x = 2\alpha^2 r^2$, $\langle N'l|V_{ho}|Nl\rangle$ can be expressed as

$$\begin{aligned}\langle N'l|V_{ho}|Nl\rangle = \frac{2\alpha^2}{m_b}\sqrt{\frac{N!}{\left(N + l + \frac{1}{2}\right)!}}\sqrt{\frac{N'!}{\left(N' + l + \frac{1}{2}\right)!}}\times \\ \int_0^\infty x^{l+\frac{1}{2}} x e^{-x} L_N^{l+\frac{1}{2}}(x) L_{N'}^{l+\frac{1}{2}}(x) dx.\end{aligned} \tag{103}$$

In this form, it is useful to employ the recurrence relations of associated Laguerre Polynomials [24]:

$$(N+1)\, L_{N+1}^{l+\frac{1}{2}}(x) = \left(2N + l + \tfrac{3}{2} - x\right) L_N^{l+\frac{1}{2}}(x) - \left(N + l + \tfrac{1}{2}\right) L_{N-1}^{l+\frac{1}{2}}(x). \tag{104}$$

By solving the recurrence relation for $xL_{N+1}^{l+\frac{1}{2}}(x)$, and using the orthogonality property of associated Laguerre Polynomials [24]

$$\int_0^\infty x^{l+\frac{1}{2}} e^{-x} L_N^{l+\frac{1}{2}}(x) L_{N'}^{l+\frac{1}{2}}(x) dx = \frac{\left(N + l + \frac{1}{2}\right)!}{N!}\delta_{N'N}, \tag{105}$$

the integral in (103) can be written as

$$I_{V_{ho}(r)} = \frac{\left(2N+l+\frac{3}{2}\right)\left(N+l+\frac{1}{2}\right)!}{N!}\delta_{N'N} - \frac{(N+1)\left(N+l+\frac{3}{2}\right)!}{(N+1)!}\delta_{N'N+1} - \frac{\left(N+l+\frac{1}{2}\right)\left(N+l-\frac{1}{2}\right)!}{(N-1)!}\delta_{N'N-1}. \tag{106}$$

Combining this expression with equations (103) and (102) allows the matrix element of the kinetic term T to be obtained

$$\langle N'l|T|Nl\rangle = \frac{2\alpha^2}{m_b}\Big[\left(2N+l+\tfrac{3}{2}\right)\delta_{N'N} - (N+1)^{\frac{1}{2}} \times \left(N+l+\tfrac{3}{2}\right)^{\frac{1}{2}}\delta_{N'N+1} - N^{\frac{1}{2}}\left(N+l+\tfrac{1}{2}\right)^{\frac{1}{2}}\delta_{N'N-1}\Big]. \tag{107}$$

Since the Cornell potential is dependent on powers of r, it is useful to find a solution to

$$\langle N'l|r^q|Nl\rangle = 2^{l+\frac{5}{2}}\alpha^{2l+3}\sqrt{\frac{N!}{\left(N+l+\frac{1}{2}\right)!}}\sqrt{\frac{N'!}{\left(N'+l+\frac{1}{2}\right)!}} \times \int_0^\infty r^{2l+2+q}e^{-2\alpha^2r^2}L_N^{l+\frac{1}{2}}\left(2\alpha^2r^2\right)L_{N'}^{l+\frac{1}{2}}\left(2\alpha^2r^2\right)dr \tag{108}$$

which can be achieved by utilising an expansion of the associated Laguerre Polynomials

$$L_N^{l+\frac{1}{2}}\left(2\alpha^2r^2\right) = \sum_{k=0}^{N}(-1)^k\frac{(N+l+\frac{1}{2})!}{k!(N-k)!(k+l+\frac{1}{2})!}\left(2\alpha^2r^2\right)^k. \tag{109}$$

Because of this expansion, the remaining integral is of Gaussian form which has a known solution

$$\int_0^\infty r^p e^{-2\alpha^2 r^2} dr = \begin{cases} \dfrac{\sqrt{\pi}(p-1)!!}{2^{p+\frac{3}{2}}\alpha^{p+1}}, & \text{for } p \text{ even} \\ \dfrac{\left[\frac{1}{2}(p-1)\right]!}{2^{\frac{p+3}{2}}\alpha^{p+1}}, & \text{for } p \text{ odd} \end{cases} \tag{110}$$

where $p = 2 + 2l + 2k + 2k' + q$. The factors of α can be taken out of this integral resulting in the expression

$$\begin{aligned} \langle N'l|r^q|Nl\rangle = & \sqrt{\frac{N!}{(N+l+\frac{1}{2})!}}\sqrt{\frac{N'!}{(N'+l+\frac{1}{2})!}} \times \sum_{k=0}^{N}\sum_{k'=0}^{N'}(-1)^{k+k'} \\ & \frac{(N+l+\frac{1}{2})!}{k!(N-k)!(k+l+\frac{1}{2})!}\,\frac{(N'+l+\frac{1}{2})!}{k'!(N'-k')!(k'+l+\frac{1}{2})!}\times \\ & (2\alpha^2)^{-\frac{q}{2}} \times I_r \end{aligned} \tag{111}$$

with

$$I_r = \begin{cases} \dfrac{\sqrt{\pi}(p-1)!!}{2^{p+\frac{3}{2}}}, & \text{for } p \text{ even} \\ \dfrac{\left[\frac{1}{2}(p-1)\right]!}{2^{\frac{p+3}{2}}}, & \text{for } p \text{ odd.} \end{cases} \tag{112}$$

The term $V(r)$ (and indeed the spin dependent term $V_{sd}(r)$) can now be calculated from equation (111) and thus the Schrödinger equation for the quenched limit can be solved. Combining the evaluated matrix elements for these terms in the Hamiltonian of the bare state, the discrete H_0 matrix can be constructed.

4.4 α Optimisation and Matrix Dimensionality

Once the matrix elements have been computed, there are two aspects of the calculation that need to be considered, namely the treatment of the harmonic oscillator parameter α and the dimensions of the matrices used. In theory, if the matrices were infinitely large α would not need to be treated because equation (87) is exact. However, since performing an infinite sum is unviable in practice, the matrix needs to be truncated and this causes α to have a significant effect on the calculation. Approximately, the value of α needs to be chosen such that the matrix elements on the diagonal are much larger than those furthest from it, otherwise matrix elements neglected due to the truncation may have a sizeable effect on the spectrum such that stable results will be unachievable when varying the size of the matrices. Although the harmonic oscillator parameter affects both aspects of the problem, for these calculations it is optimised according to the discrete spectrum only for reasons that will be discussed in due course.

α is optimised by calculating the appropriate energy eigenvalue of H_0 and varying α over a specified range, extracting the corresponding value that gives the minimum energy. Since this technique produces an overestimate, an accurate method of finding the minimum is required to give the best approximation to the true energy eigenstate. This can be achieved by writing a function that calculates the appropriate eigenvalue of H_0 and plotting over a range of values of α to find the minimum graphically. Alternatively, one can simply perform this calculation and compile the data points into a list, sorting by the lowest energy to give the minimum and thereby best value of α.

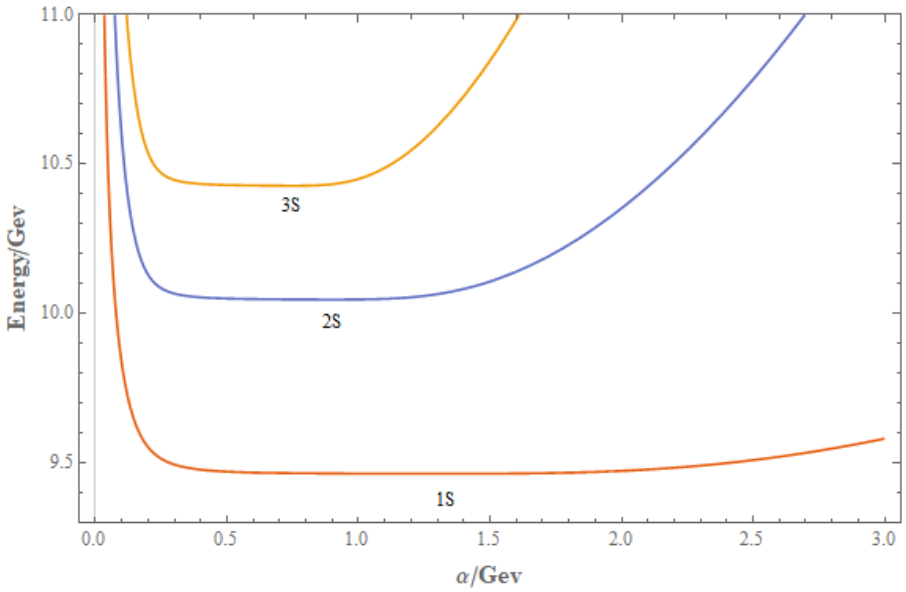

Figure 1: An example of optimising α for the $1S$, $2S$ and $3S$ states with a 15×15 matrix.

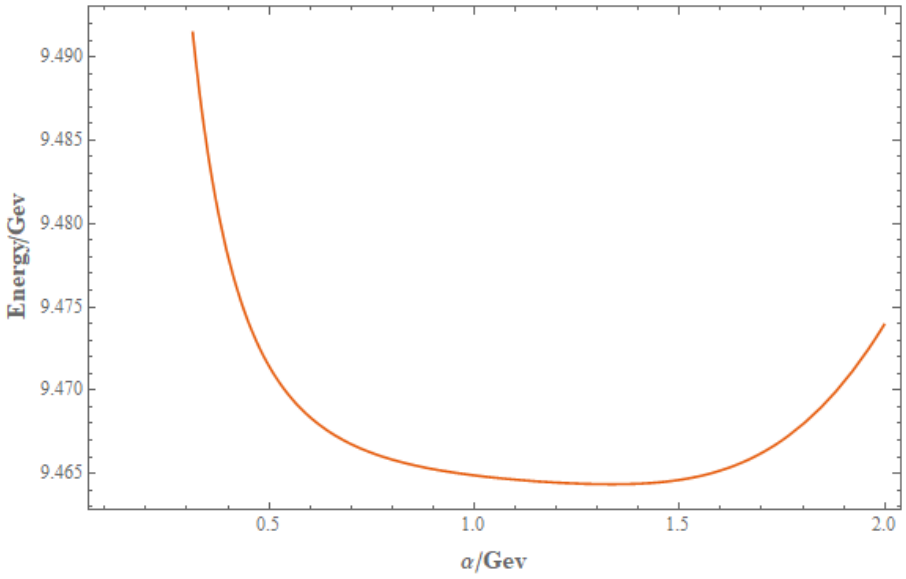

Figure 2: An example of optimising α for the $1S$ state with a 15×15 matrix.

Figure 1 displays this optimisation technique for both the ground state and

the first two excited states, indicating that higher energy levels have both a lower optimal α and smaller region of stability for the minima, which is to be expected as the error in this approximation increases with each successive excited state. From figure 1 it seems as though there is a large region of stability and hence a wide range of acceptable values for α. However, upon closer inspection the scale on the Y axis is of order 100 MeV and because this research focuses on comparing different methods of calculating the mass shifts arising from the effect on unquenching, it is imperative to be as accurate as possible to be able to draw meaningful conclusions between them, especially when the disparities are only in the order of a few MeV. Figure 2 has been scaled to 1 MeV on the Y axis for the $1S$ state and shows a stable region of roughly $1 - 1.5$ GeV for α, with both α and the minimum getting smaller with each excited state. In short, the optimal value for α (corresponding to the minima on the curve) changes for each successive energy level and the curves themselves become increasingly sensitive to α, such that the same change in this parameter results in a larger change in the Energy in excited states. It is therefore necessary to re-optimise α for each energy state and ensure the minima is selected to a suitable degree of accuracy for accurate results.

When increasing the size of the matrix, the curves in Figures 1 and 2 shift to the right, with the minima becoming flatter and wider. This is demonstrated in figure 3 by comparing the optimisation curves of the $1S$ state for $N_{\max} = 5, 15$ and 25, showing that whilst it is very important to optimise according to the state, it should also be optimised to the dimensions of the matrix as well.

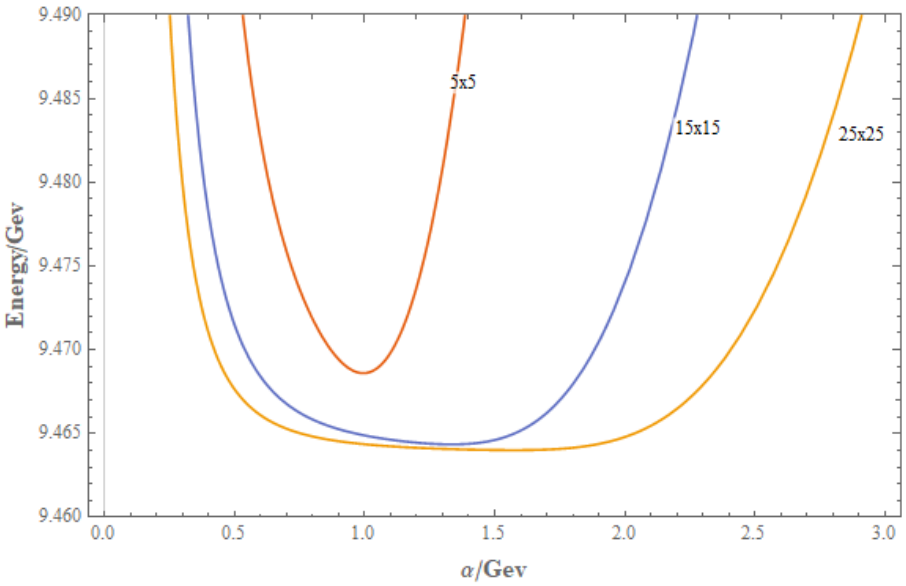

Figure 3: A comparison of optimising α for different matrix sizes in the $1S$ state.

Figure 3 also illustrates the fact that larger dimensionalities provide more stable results that are less sensitive to the harmonic oscillator parameter which is logical because more accurate approximations to equation 87 will cause the energy eigenvalues to be less sensitive to α. This feature is further exemplified in Figure 4 in which the eigenvalues of the $1S$ state are plotted against the corresponding matrix dimensions. The orange scatter plot shows this relation with α only optimised for the 4×4 matrix whilst the blue set of points show the eigenvalues when α is re-optimised at each matrix size. Both scatter curves approach stability at larger dimensions with the difference between them decreasing at each successive increase in matrix size. This behaviour is exhibited in figure 3 as the widening of the minima region essentially begins to incorporate the optimal value of α for the smaller matrices. While it is clear that larger dimensionalities provide better numerical approximations to (87), it is difficult to assign an exact uncertainty to the order of truncation. Since calculating an infinitely large matrix is impossible,

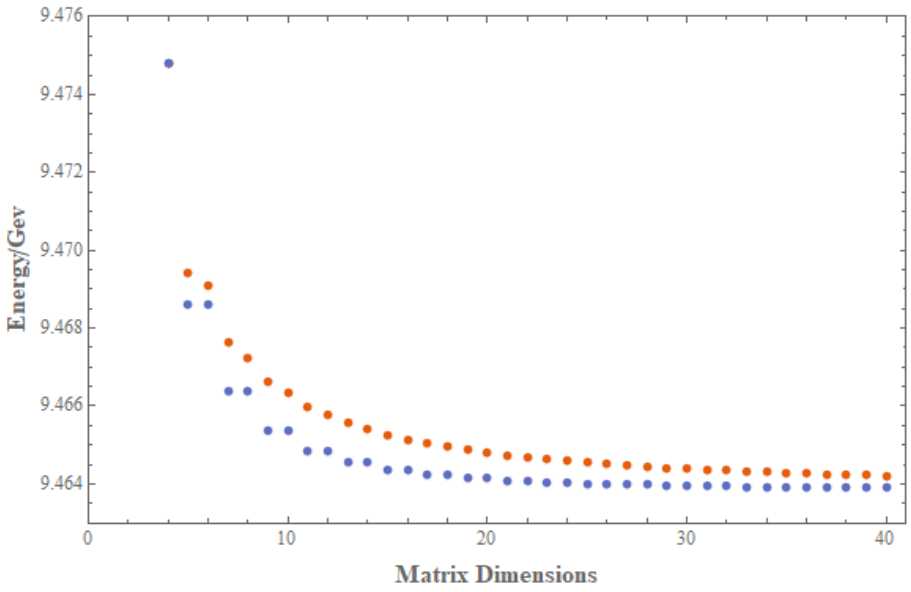

Figure 4: A comparison between optimising α for a 4×4 matrix only (orange) and for each matrix size (blue) when calculating the energy eigenvalue of H_0 in the $1S$ state.

one would need a suitably large matrix as a reference point, which has it's own uncertainty that would be different for each excited state. Furthermore, even if this could be accounted for, assigning uncertainty values to these results would be misleading as they would be calculated according to the discrete part of the problem since it would be impossible to perform for the full calculation. This would also neglect the inherent uncertainty associated with the model itself and the approximations made within it, which cannot be accurately measured.

In summary, to ensure the highest degree of accuracy for the calculations, α is optimised for both each state and matrix size, and the dimensions of the matrices themselves made as large as feasibly possible. This re-optimisation procedure is also used in other works involving the harmonic oscillator. For example, in [25] a similar technique is described in which the Hylleraas-

Undheim theorem is referenced to describe how each minimum is separately an upper bound for each energy eigenvalue, and thus tuning α to this minimum is required for a reasonable approximation. However, this does bring into question the orthogonality of the wavefunctions for the separately tuned excited states with respect to the initial ground state. In this regard, if α was constant across all considered energy levels, all of the associated wavefunctions pertaining to those states would be automatically orthogonal because they are constructed from the eigenvectors of a Hermitian matrix. However, since this is not the case, the orthogonality between the wavefunctions is not exact, but becomes exact in the limit $N_{\mathbf{max}} \to \infty$. Therefore, the orthogonality of the wavefunctions in the calculation depends on the size of the matrices used, that is, it becomes subject to the numerical accuracy of the method, which is another motivation for making the method as accurate as possible.

However, while the H_0 matrix can be made quite large with little issue, there are computational challenges with constructing the $\Omega(E)$ matrix that will be discussed later on. This is one of the reasons why α is optimised according to the discrete part of the problem because the procedure of optimising for the full spectrum would be immensely inefficient considering the number of times the optimisation would need to be repeated. Furthermore, optimising this parameter for the full spectrum is only relevant to case 4 because cases 1-3 involve calculating the eigenvalues of H_0 separately instead of forming a matrix of harmonic oscillator states and combining it with the continua spectrum. Using the same optimisation technique across all four cases is a more coherent approach seeing as the aim is to analyse the differences between each method and form conclusions based on the data acquired from the calculations. In this case, the way in which the harmonic oscillator parameter is optimised is a control across the different methods of calculation which allows a more direct comparison. Nonetheless, α does have an impact on the both aspects of the problem and it's effect on the full calculation will

also be investigated.

It is worth noting that the optimisation procedures discussed here are by no means the only ones that can be used for these calculations. For example, [1] use techniques to fit the spatial wavefunctions of the relevant state by using Gaussian expansion methods and also make simple harmonic oscillator approximations by matching $\langle r \rangle$ and maximising wavefunction overlap. It is natural that other models and methods of solving the Schrödinger equation for this problem will employ different techniques for fitting the respective wavefunctions and optimising parameters which are likely to cause some variance in results. It is also worth noting that purely numerical methods could be employed to solve this aspect of the problem without the use of basis functions and optimisation parameters, such as those mentioned in [13].

5 Matrix Elements

5.1 Building the Ω Matrix

5.1.1 Energy Denominator

Before solving, some treatment of the 'energy denominator' in the integral is required. The term $E_f(p)$ in (84) can be expressed as

$$\begin{aligned} E_f(p) &= \sqrt{m_f^2 + p^2} + \sqrt{m_f^2 + p^2} \\ &= 2m_f \sqrt{1 + \frac{p^2}{m_f^2}}, \end{aligned} \tag{113}$$

and since this project is working within the non-relativistic approximation, one can perform a Taylor series expansion where, for small x

$$\sqrt{1+x} = 1 + \frac{x}{2} - \frac{x^2}{8} + \dots. \tag{114}$$

This means $E_f(p)$ can be approximated as

$$\begin{aligned} E_f(p) &\approx 2m_f \left(1 + \frac{p^2}{2m_f^2}\right) \\ &= 2m_f + \frac{p^2}{2\mu_f} \end{aligned} \tag{115}$$

where μ_f is the reduced mass:

$$\mu = \frac{m_f m_f}{m_f + m_f} = \frac{m_f}{2} \tag{116}$$

In cases 2-4, the 'energy denominator', after the appropriate approximations, is

$$E - E_f(p) = -\epsilon - \frac{p^2}{2\mu_f} \tag{117}$$

in which ϵ is the binding energy, defined as

$$\epsilon = 2m_f - E \tag{118}$$

where

$$E < 2m_f. \tag{119}$$

The matrix element is therefore

$$\langle \hat{n}L|\Omega(E)|nL\rangle = -\sum_f C_f^2 \sum_l \int_0^\infty dp\ p^2 \frac{\mathcal{M}_l(\hat{n}L)\mathcal{M}_l(nL)}{\epsilon(m_f) + \frac{p^2}{2\mu_f}}. \tag{120}$$

It is convenient for the calculation to isolate the term for a given flavour f

$$\Omega(E) = \sum_f C_f^2 \Omega_f(E) \tag{121}$$

so

$$\langle \hat{n}L|\Omega_f(E)|nL\rangle = -\sum_l \int_0^\infty dp\ p^2 \frac{\mathcal{M}_l(\hat{n}L)\mathcal{M}_l(nL)}{\epsilon(m_f) + \frac{p^2}{2\mu_f}}. \tag{122}$$

5.1.2 Recursion Relations

With this integral, a solution has been found for the $n = 0$ case. However, in order to build the matrix $\langle \hat{n}L|\Omega(E)|nL\rangle$, a method of obtaining the $n = 1, 2 \ldots N_{\max}$, and indeed $\hat{n} = 1, 2 \ldots N_{\max}$, cases is required for an $N_{\max} \times N_{\max}$ matrix. Fortunately, due to orthogonality properties of the Laguerre Polynomials found in the harmonic oscillator wavefunctions of the

discrete states, one can construct recursion relations between them relating the ground state to those of higher order. This property was originally derived in [26]. The recursion relation is defined as

$$\begin{aligned}\langle r|nL,\alpha\rangle = &\sqrt{\frac{(n-1)\left(n+L-\frac{1}{2}\right)}{n\left(n+L+\frac{1}{2}\right)}}\langle r|n-2,L,\alpha\rangle \\ &+\frac{1}{\sqrt{n\left(n+L+\frac{1}{2}\right)}}\alpha\frac{d}{d\alpha}\langle r|n-1,L,\alpha\rangle\,.\end{aligned} \tag{123}$$

The spatial factors, $\mathcal{M}_l(nL)$, given in [2] have a dependence on both harmonic oscillator parameters α and β of the initial and final state mesons respectively. However, since the recursion relation involves a differential with respect to α, it is necessary to make this dependence explicit by making α an argument of the function:

$$\mathcal{M}_l(nL) \to \mathcal{M}_l(nL,\alpha). \tag{124}$$

Thus, the recursion relation becomes

$$\begin{aligned}\mathcal{M}_l(nL,\alpha) = &\sqrt{\frac{(n-1)\left(n+L-\frac{1}{2}\right)}{n\left(n+L+\frac{1}{2}\right)}}\mathcal{M}_l(n-2,L,\alpha) \\ &+\frac{1}{\sqrt{n\left(n+L+\frac{1}{2}\right)}}\alpha\frac{d}{d\alpha}\mathcal{M}_l(n-1,L,\alpha).\end{aligned} \tag{125}$$

For the treatment of (122), one option would be to obtain the required spatial factors from the recursion relations and then integrate to obtain the matrix element. However, it would be convenient, not to mention more computationally efficient, to apply the recursion relation outside the integral to avoid needlessly computing different integrals for each element in the matrix. To do this, one must distinguish the oscillator parameters for the $|nL\rangle$ state (α) and the $|\hat{n}L\rangle$ state ($\hat{\alpha}$) to apply the recursion relation to them separately,

and so (122) becomes

$$\langle \hat{n}L|\Omega_f(E)|nL\rangle = -\sum_l \int_0^\infty dp\ p^2 \frac{\mathcal{M}_l(\hat{n}L,\hat{\alpha})\mathcal{M}_l(nL,\alpha)}{\epsilon(m_f)+\frac{p^2}{2\mu_f}}. \tag{126}$$

This is an incredibly powerful feature because for a given L, one can simply compute the integral once for the $n = \hat{n} = 0$ case and all other matrix elements can be deduced using the appropriate recursion relation from

$$\begin{aligned}\langle \hat{n}L|\Omega_f(E)|nL\rangle = &\sqrt{\frac{(n-1)\left(n+L-\frac{1}{2}\right)}{n\left(n+L+\frac{1}{2}\right)}}\,\langle \hat{n}L|\Omega_f(E)|n-2,L\rangle \\ &+\frac{1}{\sqrt{n\left(n+L+\frac{1}{2}\right)}}\alpha\frac{d}{d\alpha}\,\langle \hat{n},L|\Omega_f(E)|n-1,L\rangle\end{aligned} \tag{127}$$

and

$$\begin{aligned}\langle \hat{n}L|\Omega_f(E)|nL\rangle = &\sqrt{\frac{(\hat{n}-1)\left(\hat{n}+L-\frac{1}{2}\right)}{\hat{n}\left(\hat{n}+L+\frac{1}{2}\right)}}\,\langle \hat{n}-2,L|\Omega_f(E)|nL\rangle \\ &+\frac{1}{\sqrt{\hat{n}\left(\hat{n}+L+\frac{1}{2}\right)}}\hat{\alpha}\frac{d}{d\hat{\alpha}}\,\langle \hat{n}-1,L|\Omega_f(E)|nL\rangle\,.\end{aligned} \tag{128}$$

In other words, an entire spectrum of states can be calculated by merely solving one integral and applying two relations (of the same structure) to it, allowing a large number of states to be considered in the calculation automatically. This arises from the inherent orthogonality of the harmonic oscillator states and such properties can be a highly useful tool in these types of numerical computations. However, there are several ways in which these recursion relations can be implemented into the building of the matrix which have been studied to maximise efficiency in the construction of the matrix. These ideas will be briefly discussed presently.

5.1.3 Solving the Integral

In order to begin building the matrix, it is necessary to solve the integral in (126) by finding solutions of

$$I = \int_0^\infty dp\ p^2 \frac{|\mathcal{M}_l|^2}{\left(\epsilon + \frac{p^2}{2\mu}\right)} \tag{129}$$

where, for harmonic oscillator wavefunctions, $\mathcal{M}_l$ can be expressed as

$$\mathcal{M}_l = e^{-ap^2} p^l \sum_k^K C_k p^{2k} \tag{130}$$

by virtue of the spatial factors presented in [2]. From this, it can be deduced

$$|\mathcal{M}_l|^2 = e^{-2ap^2} p^{2l} \sum_{kk'}^K C_k C_{k'} p^{2k+2k'}. \tag{131}$$

Thus, the integral can now be defined as

$$I(a, m, \epsilon, \mu) = \int_0^\infty dp\ \frac{p^{2+2m} e^{-2ap^2}}{\left(\epsilon + \frac{p^2}{2\mu}\right)} \tag{132}$$

where $m = l + k + k'$. Performing a change of variables with the substitution $x = p^2$ gives

$$I(a, m, \epsilon, \mu) = \frac{1}{2\epsilon} \int_0^\infty dx\ \frac{x^{m+1/2} e^{-2ax}}{\left(1 + \frac{x}{2\mu\epsilon}\right)}. \tag{133}$$

However, it is necessary to perform a second change of variables by substituting $t = \frac{x}{2\mu t}$, giving

$$I(a, m, \epsilon, \mu) = \frac{(2\mu\epsilon)^{m+3/2}}{2\epsilon} \int_0^\infty dt\ \frac{t^{m+1/2} e^{-4a\mu\epsilon t}}{(1+t)} \tag{134}$$

which is very similar in form to the confluent hypergeometric function of the second kind in [27], defined as

$$U(f,b,z) = \frac{1}{\Gamma(f)} \int_0^\infty dt\ e^{-zt} t^{f-1} (1+t)^{b-f-1} \tag{135}$$

where $\Gamma(f) = (f-1)!$. This is exactly the same integral as in (134) with $z = 4a\mu\epsilon$, $f = m + \frac{3}{2}$ and $b = m + \frac{3}{2}$, thus

$$I(a,m,\epsilon,\mu) = \frac{\Gamma\left(m+\frac{3}{2}\right)}{2\epsilon} (2\mu t)^{m+\frac{3}{2}} \times U\left(m+\tfrac{3}{2}, m+\tfrac{3}{2}, 4a\mu t\right). \tag{136}$$

5.2 Specifying the Considered Transition

The spatial factor $\mathcal{M}_l(nL,\alpha)$ is defined in [2] as

$$\mathcal{M}_l(nL,\alpha) = \frac{\gamma}{\sqrt[4]{\pi}} \exp\left(-\frac{p^2(r-1)^2}{2\alpha^2+\beta^2}\right) \mathcal{A}_l(nL,\alpha) \tag{137}$$

where γ is a coefficient relating to the effective strength of the pair creation and $r = \frac{m_q}{m_q+m_b}$, in which m_q is the created quark mass (m_u, m_d or m_s) and m_b the mass of bottomonium. $\mathcal{A}_l(nL,\alpha)$ is a factor dependent on the type of transition considered for the calculation and β is the oscillator parameter of the final state mesons, which in this work is taken to be 0.4 GeV as is frequently adopted in the literature [2,28,29]. This equation allows the factors relating to the state's spatial wavefunction to be computed and combined with the flavour and angular momentum coefficient in (76) to calculate the overall matrix element in (16).

At this stage, it is important to emphasise that the framework put forward for the calculations in this thesis so far are general in form, and as such can be used for any L wave transition by appropriating the relevant factor from [2]. This paper lists both the factors and coefficients needed to calculate each spin

permutation of the S,P,D,F and G transitions. However, the focus of this thesis will be on the $nS \to 1S + 1S$ which, due to the spin approximations made in section 3, averages over all of the transitions in the multiplet, for example, ${}^3S_1 \to {}^1S_0 + {}^1S_0$, ${}^3S_1 \to {}^3S_1 + {}^1S_0$ etc... Thus, $\mathcal{A}_l(nL, \alpha)$ can be defined:

$$\mathcal{A}_P(1S, \alpha) = \frac{-8p\alpha^{3/2}\left(2r\alpha^2 + \beta^2\right)}{\sqrt{3}\left(2\alpha^2 + \beta^2\right)^{5/2}}. \tag{138}$$

In addition, for this transition amplitude, the pertinent spatial factor coefficient is $\sqrt{12}$. Therefore, the overall expression for the seed matrix element $n = \hat{n} = 0$, from which all other states are derived via the recursion relations (127) and (128), is

$$\begin{aligned}\langle 1S|\Omega_f(E)|1S\rangle = &-\frac{2^8\gamma^2\Gamma\left(\frac{5}{2}\right)}{2\epsilon\sqrt{\pi}}\frac{\alpha^{3/2}\left(2r\alpha^2 + \beta^2\right)}{\left(2\alpha^2 + \beta^2\right)^{5/2}}\frac{\hat{\alpha}^{3/2}\left(2r\hat{\alpha}^2 + \beta^2\right)}{\left(2\hat{\alpha}^2 + \beta^2\right)^{5/2}} \\ &\times (2\mu\epsilon)^{\frac{5}{2}}\ U\left(\frac{5}{2}, \frac{5}{2}, 2\mu\epsilon\left(\frac{(r-1)^2}{2\alpha^2 + \beta^2} + \frac{(r-1)^2}{2\hat{\alpha}^2 + \beta^2}\right)\right).\end{aligned} \tag{139}$$

It is important to note that since the matrix has been isolated for a given flavour f, when the calculation is being considered for up/down quarks there is an additional factor of 2 in the equation. This is because there is a sum over contributions from B^+B^- and $B^0\bar{B}^0$, and since it is assumed these are degenerate, the contributions are identical and thus effectively multiplied by 2. Furthermore, when the strange quark variation is being calculated, the effective strength of the pair creation is replaced with $\gamma_s = \left(\frac{m_q}{m_s}\right)\gamma$.

5.3 Computational Techniques and Efficiency

When building the $\Omega(E)$ matrix, there are many different approaches one can take to implement the recursion relations once the initial $(1, 1)$ element has been computed. For example, a simple approach would be to calculate the first column in the matrix and use the recursion relations to fill out the rest

or vice versa. However, since equations (127) and (128) are equal, the matrix is symmetric about the diagonal and therefore only one half of the elements actually need to be calculated. In addition, another simplification is made in which the elements furthest from the diagonal are made to be zero to further reduce the computation time. This is not only a reasonable approximation to make, but a beneficial one because the elements lying furthest from the diagonal are orders of magnitude smaller than those on it and sacrificing them allows larger matrix structures to be evaluated per unit time which is important for both accurate and stable results. To check this, the full calculation was conducted for $\delta = 4$ and $\delta = 6$, using 10×10 matrices, where δ is the number of off diagonal elements in the matrix and no discernable difference was found in the mass shift. This essentially becomes a trade off between computing more elements on and around the diagonal or those furthest away that contribute comparatively little to the calculation and so restricting the matrices to $\delta = 4$ is a sensible numerical decision in this context.

Careful consideration of the way in which the derivatives are implemented in the recursion relations is also essential for efficient computation of the matrix elements. It was found that directly inputting (139) into the (1,1) element and taking derivatives of that expression was extremely cumbersome and consequentially took hours to form even relatively small matrices. To solve this issue, a generic, undefined function $f^{(0,0)}(\alpha', \alpha)$ was inserted into the starting element and the recursion relations were applied. This resulted in the matrix elements simply being constructed in terms of various combinations of $f^{(j',j)}(\alpha', \alpha)$, multiplied by the appropriate coefficients and factors of α and α', as a consequence of the chain rule in the derivatives. For example, the (1,3) element of the matrix would constitute a combination of $f^{(0,0)}(\alpha', \alpha)$, $f^{(0,1)}(\alpha, \alpha')$ and $f^{(0,2)}(\alpha', \alpha)$. Subsequently, once the matrix has been built in terms of these functions, $f^{(0,0)}(\alpha', \alpha)$ is then replaced with (139). The benefit of this approach is that each iteration of $f^{(j',j)}(\alpha', \alpha)$ is only computed once

and therefore when it is used within the expressions of the proceeding matrix elements, it is evaluated instantly. This significantly reduced computation time allowing larger matrix structures to be realised which is essential for accuracy in these numerical calculations.

Other techniques included making a distinction between the first two arguments of the hypergeometric function in (136) by inputting m' as one of them and then only evaluating m and m' after the matrix had been constructed. This was necessary because *Wolfram Mathematica* simplifies the hypergeometric into an exponential and an incomplete gamma function when it's first two arguments are identical. As a result, the recursion relations were then taking derivatives of a product of two functions which is significantly more computationally intensive than simply differentiating $U(f, b, z)$:

$$\frac{d}{dz}U(f, b, z) = -fU(f + 1, b + 1, z). \tag{140}$$

Lastly, when calculating cases 3 and 4, equations (44) and (66) are plotted by varying E over a specified range and finding the relevant intercepts that satisfy the respective equations. The challenge with this is the $\Omega(E)$ matrix becomes time consuming to construct at large dimensions and so recomputing it for many energy values is not feasible. However, as shown in figure 6, the functions plotted have an approximately linear relationship and therefore the number of plot points can be restricted without seriously compromising the shape or intercepts of the graph. To improve the accuracy and validity of this approximation, the plot range was reduced so that the points being calculated were close to the intercept. In the final calculations, 4 data points were considered and despite these computational challenges only really applying to cases 3 and 4, this was also implemented in solving case 2 for consistency when comparing data.

6 Results and Discussion

6.1 Methods of Calculation

Before analysing the mass shift data pertaining to each of the four cases discussed in section 2, the methods by which they were implemented into *Wolfram Mathematica* will be discussed. Firstly, the calculation for case 1 involved constructing H_0, using the optimisation procedure outlined in section 4.3, and extracting the relevant eigenvalue to obtain the bare mass M_n. Then, the mass shift is calculated by building $\Omega(M_n)$ using the seed integral and recursion relations in section 5 and inputting the bare mass as indicated in equation (35), taking the applicable element from the diagonal depending on the state being evaluated. Case 2 is similar in the sense that the bare mass is calculated from H_0 and the mass shift is taken from the applicable element on the diagonal, except the continuum matrix, $\Omega(E)$, now has energy as the argument thus forming a transcendental equation, as expressed in (40). To solve this, the matrix element is taken to the left hand side of equation (40) and the energy is varied over a specified plot range to observe the intercept. As well as this, $M_n - E$ is also plotted over the same range and the difference between the two intercepts is the mass shift, as illustrated in figure 5. Cases 3 and 4 are also solved in a similar fashion through varying the energy and finding graphical solutions that satisfy the respective equations. However, the solution to equation (55) requires building the full $\Omega(E)$ matrix and performing a dot product with the eigenvectors of H_0, before combining it with the relevant eigenvalues to find a graphical solution. In contrast, the mass shift in the context of case 4 is calculated by forming the full H_0 and $\Omega(E)$ matrices, summing them to form $\mathcal{H}(E)$ and plotting the determinant as outlined in equation (66) while varying the energy, as depicted in figure 6.

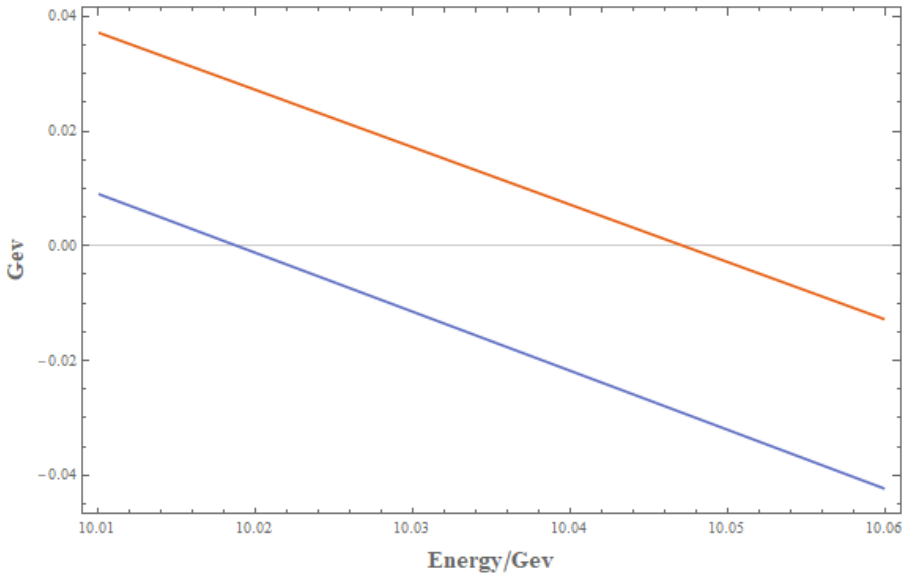

Figure 5: A plot of equation (40) against energy for a 15×15 matrix in the $1S$ state. The orange line represents $M_n - E$ whilst the blue line denotes the corrected mass once the unquenching effects are taken into account, with the points of intersection providing a solution to (40)

When plotting to find graphical solutions in this way, it is imperative to ensure that stable results are achieved when varying the control parameters α and $N_{\max}$. Since these parameters are intrinsically related to one another, the optimisation technique outlined in section 4.3 was conducted in which α was re-calculated, and graphs plotted, for each matrix size. The intercepts and overall mass shifts were then analysed in each plot when varying $N_{\max}$ from 4 to 15. As expected, the respective intercepts and mass shifts experienced the most change between lower dimensionalities, beginning to stabilise at values of approximately 10 or larger for $N_{\max}$, which roughly coincides with figure 4. To ensure confidence in all of the results attained, this procedure was repeated for each state and case being considered. The set of data presented in 2 uses 15×15 matrices as this was found to be the best compromise between accuracy and viability of the calculation since it provides stable results and the best approximation to (87) whilst still being computationally viable.

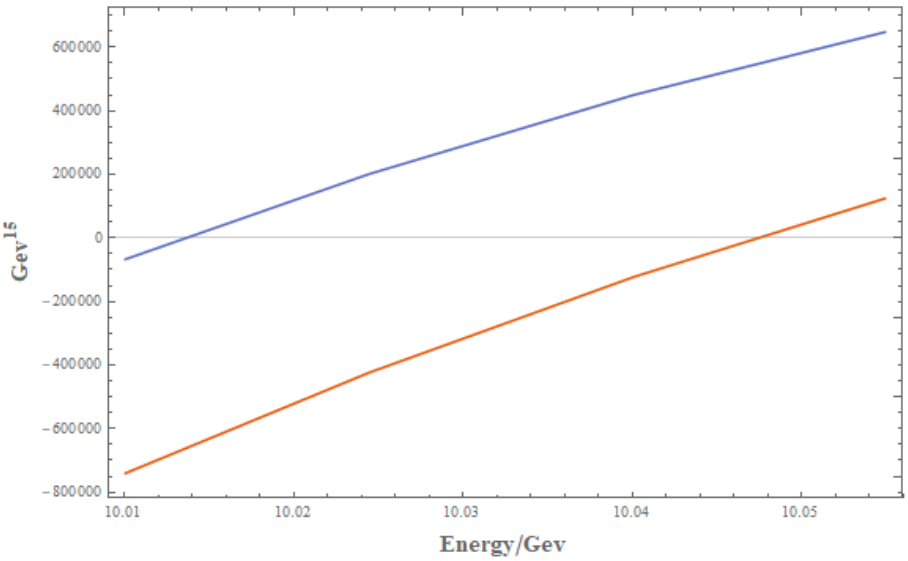

Figure 6: A plot of the left hand side of equation (66) against energy for a 15×15 matrix in the $2S$ state, representing the full calculation for case 4. As before, the orange line denotes the bare mass and the blue line the corrected mass once the unquenching effects are considered.

Continuing the discussion in section 4, the effect of α on the full calculation was also investigated to see the extent it influences the mixing matrix which determines the mass shift due to unquenching. This was implemented by plotting for case 4 in the $2S$ state, but with one plot optimised appropriately and another using the value of α for the $1S$ state.. Comparing figures 6 and 7, for which the values of α are 0.903 GeV and 1.335 GeV respectively, it is evident that neglecting to re-optimise the harmonic oscillator parameter causes a notable difference in not only the point of intersection with the x axis, but also the mass shift itself. In this case the difference is approximately 3.5 MeV which is an error of $\sim 10\%$ and this disparity is even larger when considering the $3S$ state.

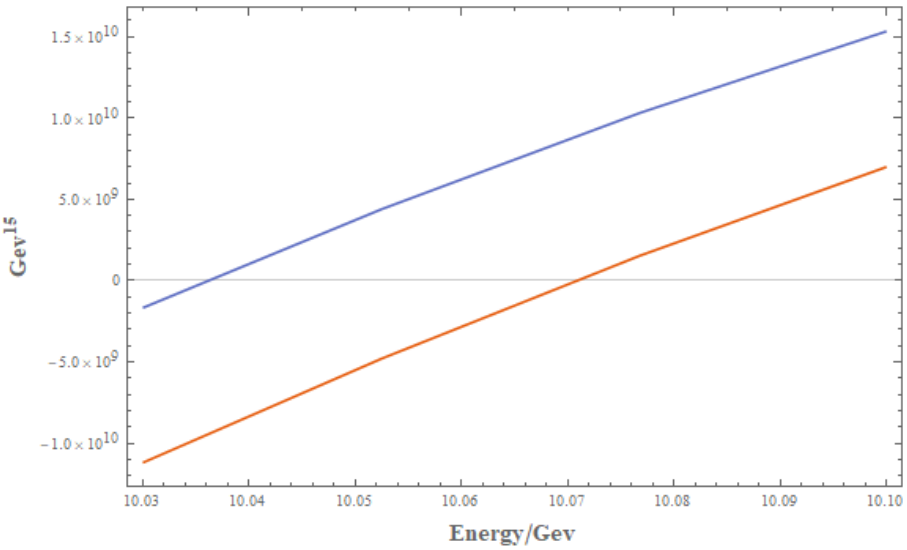

Figure 7: A repeat of the plot in figure 6 but with α optimised for the $1S$ state instead of appropriately for the $2S$.

Since this research focuses on comparing different methods of calculating the problem, it is crucial to be as accurate as possible in each variation of the method to be able to draw any meaningful conclusions between them, especially when the differences in the mass shift of the separate cases is the order of the error just mentioned. Therefore, when controlling optimisation parameters it is imperative to have a reliable and repeatable procedure that can be applied to all the relevant cases to ensure that each set of data can be compared justly. For these reasons, it is not suitable to simply optimise α once and use that value for other energy states or matrix dimensions, particularly if those dimensions are relatively small.

6.2 Mass Shift Data

State			**1S**	**2S**	**3S**
$\boldsymbol{M_n}$/MeV	H_0		9464.4	10047.2	10427.9
	[1]		9465.6	10047.2	10427.6
$-\boldsymbol{\Delta M}$/MeV	Case 1	B	14.6	29.2	49.0
		B_s	5.5	8.6	11.1
		Total	**20.1**	**37.8**	**60.1**
	Case 2	B	14.5	28.4	44.6
		B_s	5.5	8.6	11.0
		Total	**20.0**	**37.0**	**55.6**
	Case 3	B	17	33.6	37.5
		B_s	5.3	8.2	7.8
		Total	**22.3**	**41.8**	**45.3**
	Case 4	B	16.8	33.8	36.3
		B_s	5.5	8.8	8.1
		Total	**22.3**	**42.6**	**44.4**
	[1] GEM	B	15.85	33.025	48.525
		B_s	6.75	10.4	10.725
		Total	**22.6**	**43.425**	**59.25**
	[1] SHO	B	15.85	32.25	42.225
		B_s	6.75	10.225	9.825
		Total	**22.6**	**42.475**	**52.05**
$\boldsymbol{M_{\mathbf{exp}}}$/MeV	[3]		9444.9	10017.2	n/a

Table 2: Spin-averaged mass shifts caused by the effect of unquenching for the $1S$, $2S$ and $3S$ states. M_n denotes the bare mass of the Cornell potential, the parameters of which are taken from [1], and $-\Delta M$ the mass shift for each of the four cases discussed in section 2 as well as the two methods presented in [1]. $M_{\mathbf{exp}}$ represents the experimentally obtained values where applicable from [3] and B and B_s the spin-averaged contributions to the total mass shift from the B and strange B mesons respectively.

Table 2 contains the bare mass and mass shift results for each of the four cases in the $1S$, $2S$ and $3S$ states, as well as corresponding data from [1] pertaining to the two methods discussed in the paper. GEM denotes the Gaussian expansion method of solving the problem whilst SHO denotes a

simple harmonic oscillator approximation to the wavefunction by matching $\langle r \rangle$ and maximising wavefunction overlap. These results from [1] have been spin-averaged using the model

$$nS = \frac{1}{4}\left(n^1S_0 + 3\ n^3S_1\right) \tag{141}$$

so that it can be compared. Also included for reference are the experimentally obtained values where possible, that have also been spin-averaged using the above. It should also be noted that data was collected and checked against that of [2], using their parameter selection, for each of the cases in table 2. However, in this thesis α is not optimised, with a constant value of the harmonic oscillator parameters for both initial and final state mesons across all states. For this reason, while the data set was useful for checking the calculation using this value of α (for which results were in agreement to within a few MeV), it is not suitable for direct comparison with the data collected in 2 due to the optimisation procedures outlined in section 4.3 as this produced results that differed significantly. For example, the total spin-averaged mass shift for the $1S$ state in [2] was 57.6 MeV whilst the corresponding value in each of the four cases was between 44-46 MeV, and this disparity increased for higher lying states.

Comparing the data for M_n, the masses obtained via the extraction of eigenvalues from H_0 are very similar to those obtained from spin averaging the figures included in [1] according to (141). The $1S$ state contains the largest difference of only 1.2 MeV, with the $2S$ identical and the $3S$ showing a mere 0.3 MeV disparity to 1dp. The fact that these figures are so similar is somewhat expected considering the same potential and parameters were used in the model. However, it is also encouraging since [1] uses Numerov's method [30] in solving the Schrödinger equation to obtain the discrete wavefunctions, whereas in this work they are acquired via an expansion

in harmonic oscillator basis functions. This shows reproducibility between the different approaches and again highlights the importance of optimising the harmonic oscillator parameter and using suitable matrix dimensions to achieve stable results for the bare mass.

Analysing the mass shift data for the $1S$ state, the values given by [1] are exactly identical in both the Gaussian expansion method and the simple harmonic oscillator approximation, at 22.6 MeV, with no variation in the B and B_s components. This therefore suggests that SHOs are a good approximation to the real wavefunctions in determining the mass shift for the ground state energy level. Cases 3 and 4 are congruent with these results, only off by 0.3 MeV for the overall change in mass. However, they do include a noticeably different weighting for the B and B_s variations with the strange B mesons contributing to a lower proportion of the total mass shift than in the cases put forth in [1]. In contrast, cases 1 and 2 both produce a lower change in mass of about 20 MeV, but interestingly have similar contributions for the B_s mesons as cases 3 and 4. This is inconsistent, albeit only slightly, with the comparison of GEM and SHO methods since cases 1 and 2 effectively assume simple harmonic oscillator wavefunctions at the point of coupling and find the mass shift reduced by approximately 2.3 MeV, so while this is a reasonable approximation, it is not found to be as accurate as the methods presented in [1] suggest. Also, comparing the incorporated mass shift to the experimental value, it is very similar in all four cases.

This pattern is further exemplified in the $2S$ state, as the SHO approach provides a compelling approximation to the GEM, having a lower mass shift by only 0.95 MeV. However, comparing the first two cases to 3 and 4 the difference is much larger, between 4 and 5.6 MeV, with the largest disparity from cases 2 and 4, indicating that simple harmonic oscillators provide a less accurate approximation to the wavefunction at higher energy levels. Furthermore, there are now also noticeable differences between all of the approaches.

Case 1 which is derived using techniques in leading order perturbation theory has a slightly larger downward mass shift than Case 2 which is solved self consistently in a coupled channel approach. In addition, there is also a 0.8 MeV difference between cases 3 and 4. While both of these approaches make use of the full $\Omega(E)$ matrix, the discrete component of the wavefunction in case 3 is an eigenstate of H_0 whereas in case 4 it is a mixture of eigenstates. There are also larger disparities in comparison to the experimental data for this state, but the mass shifts are the correct order of magnitude showing approximately a 10 MeV difference in the renormalised mass.

Inspecting the $3S$ data, the disparity in the mass shift results across the various approaches is much larger than in the lower two energy levels. Comparing the GEM and SHO methods in [1] for this state, the simple harmonic oscillator wavefunction approximation is significantly less accurate than in the previous states, producing a lower mass shift by 7.2 MeV. Furthermore, larger differences are also seen between the four cases, with a 4.5 MeV smaller mass shift in case 2 compared to case 1 and a 10.3 MeV disparity between cases 2 and 3. This is congruent with [1] in that the discrepancy in mass shift between SHOs and well approximated wavefunctions increases for higher lying states, and also highlights the limits of perturbation theory as a viable approach to the problem at higher energy levels. However, the pattern in which these differences arise has changed for the $3S$. Whilst case 1 shows a larger mass shift than case 2 across all three states, the absolute change in mass then consistently increases between cases 2, 3 and 4 in the $2S$ state. This trend is then reversed when considering the $3S$ as the mass shift increases significantly for cases 1 and 2 and less so for the following two approaches, resulting in case 4 producing the largest mass shift for the $2S$ state and the smallest mass shift for the $3S$ state. This is somewhat inconsistent with the findings of [1] as the Gaussian expansion method experiences both a larger change in mass than the simple harmonic oscillator approximation and a larger change in it's mass shift from the $2S$ to $3S$ states.

While these figures are very useful as a point of reference and comparison, differences in the simplifications made, techniques by which the wavefunctions are approximated and methods of finding a solution to the Schrödinger equation are likely to have a larger impact at higher energy levels. This is due to the energy denominator in (16) because when $E_\lambda(p) - E$ is small, the argument of the integral becomes large and therefore the elements of $\Omega(E)$ which determine the mass shift are sensitive at near threshold states. Thus, it is possible that some aspect of the respective calculations that cause a small change to $E_\lambda(p)$ or E could potentially translate to sizeable effects on the overall mass shift near threshold. For example, in section 3.2 an approximation was made in which the continuum mesons were restricted to S-wave, radial ground states, i.e. $n_1 = n_2 = 0$ and $L_1 = L_2 = 0$. While a similar approximation was made in [1] regarding the radial ground states of mesons in the continuum, the orbital angular momentum was not restricted in this way and thus 'coupled channel induced S-D mixing' was taken into account in their calculations. Although the largest contributions to $\Omega(E)$ arise from the continua with the smallest masses, it could be possible that neglecting S and D wave channel mixing has had some effect on the mass shift for the $3S$ state.

Since the discrete wavefunction is expanded in the Gaussian basis in [1], the oscillator parameters are set to be a geometric series [31] and varied to fit the wavefunction. This fitting via oscillator parameters is also how the SHO approximation is made by maximising wavefunction overlap [28] and matching $\langle r \rangle$ [32–34]. Not only is this a different approach to the optimisation procedures discussed in section 4, but it follows that different values for these parameters would be used in the GEM and SHO methods, whereas the same values are used across all four cases in table 2. An analogous approach to the SHO fitting would be to vary α until the eigenvectors had maximum overlap with those of the simple harmonic oscillator. This contrast in approaches to fitting the oscillator parameters could also have contributed to the differences

seen in table 2 for the total mass shift in the $3S$ state. However, since the primary aim of this work is to analyse the effect variations in each method have on the mass shift, it makes more sense to work under a common set of parameters, including α.

7 Summary and Conclusions

The data gathered in table 2 suggests a simple harmonic oscillator approximation at the point of coupling between the discrete and continuum components of the wavefunction is somewhat reasonable for ground state energy levels, but diverges with less consistent results at higher lying states. In addition, within this approximation, there are noticeable differences between the coupled channel setup and perturbative approaches to the problem in the 3S state. This could indicate that the assumption of treating the coupling term U in the Hamiltonian, which is responsible for mixing between valence and continuum states, as a small effect in comparison to H_0 becomes less valid near threshold. This is consistent with the theory because the denominator in (35) becomes smaller when the bare mass is large and thus induces a larger effect on the mass shift, representing a higher opportunity for coupling between valence and continuum mesons. Furthermore, the data collected also indicates that treating the discrete component of the wavefunction as a mixture of eigenstates of H_0 (as in case 4) as opposed to a single eigenstate of H_0 has a negligible effect at the ground state, but does show some small disparities at higher energy levels. This suggests that the coupling between different valence states due to meson loops is a small effect that becomes more significant towards threshold energies. This mixing of discrete eigenstates, which themselves are mixtures of harmonic oscillators, seems to slightly increase the mass shift at the 2S level, but suppress it at the 3S, possibly indicating that mixing valence states reduces the change in mass due to unquenching

near threshold. Nonetheless, since the differences between cases 2 and 3 are quite small, one can not be assured in this conclusion.

These cases also correlated well with the results of [1] for the 1S and 2S levels, but differed fairly significantly for the 3S state. However, as previously discussed this could be due to the variations in approaches, approximations and assumptions made, such as the restriction of orbital angular momentum for continuum mesons, which are likely to be amplified at near threshold energies. In summary, the results presented in this thesis show that across the four cases studied, the largest effect on the mass shift stems from the proper treatment of the discrete wavefunction and therefore should be a necessary inclusion in these types of calculations, particularly near threshold, a conclusion shared by [1].

While the incorporation of mixing between discrete eigenstates, as presented in (66), is only shown to have a small effect in the $2S$ and $3S$ states in table 2, this does not necessarily translate for other wave transitions and therefore provides an opportunity for further research in this field. Moreover, the calculations themselves would be fairly straightforward to set up because it simply involves changing the l dependent parameters in the discrete spectrum and adjusting the seed integral in $\Omega(W)$ using the appropriate spatial factors and angular momentum coefficients from [2] and [17] respectfully. In addition, the solution to the integral is identical regarding the confluent hypergeometric function, the only difference being the coefficients and powers of p depending on the particular wave transition being calculated. From this, the recursion relations are applied in the same way and thus $\Omega(W)$ can be built and the full calculation solved for other values of L. In cases involving $L > 0$, there is not one, but two partial waves, for example, a $P \to S + S$ transition goes in both S and D wave. This does not fundamentally change anything in the calculation, but may become increasingly numerically intensive as each element is more algebraically complicated. One would expect

larger mass shift effects in states with $L > 0$, for example in [1] the P wave transitions experienced at least a further 10 MeV shift compared to the S wave states.

Investigating the behaviour of this mixing on the mass shift for multiple transition amplitudes is a worthwhile endeavour because it's possible that this effect is not as small as the $nS \to 1S + 1S$ transition in such cases and therefore should be an important factor in these calculations when trying to establish accurate models for the unquenched system. Conversely, if this effect is indeed small across all transition amplitudes then it is nonetheless useful information to have when considering the requirements of the models and methods needed for computing these mass shifts. However, since this approach solves both the discrete and continuum parts of the problem simultaneously, it can be argued that it is an advantageous technique anyway as it does not require the discrete wavefunctions to be calculated separately and re-inserted into the continuum matrix, and the inclusion of mixing between discrete eigenstates is an added benefit from the setup. Also, it would be interesting to see if the effect of suppressing the mass shift near threshold implied by the data in table 2 is consistent among the other transition amplitudes.

Since the approximations made in section 3 are not essential to compute the change in mass due to unquenching, the calculations presented in this paper could be taken even further to include spin splittings and non-restricted continuum mesons. Including these features of the model would allow a more direct comparison to data in papers such as [1] and also warrant the use of $V_{sd}(r)$ in the discrete Hamiltonian, therefore negating the need for equation (141). In addition, spin-averaging as an approximation is known to become less accurate near threshold and thus differences between the two approaches could be analysed in this energy region to quantify the effect it may have on the mass shift. As well as this, not restricting continuum mesons to $L_1 =$

$L_2 = 0$ could allow mixing between states of different angular momentum which may also have an effect on the observed change in mass. Quantitative analysis could be undertaken between the various sets of approximations to determine the relative impact each of them have on the results of the model.

Other areas that could be investigated include the optimisation of the harmonic oscillator parameter because the technique proposed in this thesis involved tuning it according to the discrete spectrum, but an equally valid approach could involve varying α with the full calculation and finding the minimum. However, the problem with this is the computational intensity associated with constructing $\Omega(E)$, particularly if the aforementioned approximations are not implemented, and therefore the time it would take to re-optimise for each state and matrix size. Similarly, the matrices themselves could arguably be extended to greater dimensionalities for a more accurate wavefunction, but considering the exponential relationship between increasing $N_{\max}$ and computation time observed during calculation, at a certain point the benefits of increasing accuracy begin to have diminishing returns. This then raises an interesting point about the role these models have in QCD because if they are being used, it is within the field's interest to make them as accurate as possible. But with that being said, since the potential models are inherently approximate anyway, increasing accuracy to the point of huge computation times may be redundant when there are alternative approaches such as Lattice QCD that encapsulate the Physics to a higher standard, particularly when a primary benefit of using models over Lattice QCD is the significantly reduced calculation work.

One interesting approach to accounting for unquenching effects without direct computation of the valence-continuum coupling could involve an investigation into the potential model parameters to discern whether they can be adjusted to incorporate the reduction in mass. This could be achieved by first fixing the initial parameters for the bare state as given in other works

or through some rationale, for example, fitting the various state masses to experimental data, such as those in [35], or indeed fitting the wavefunction to dielectric decay widths as is done in [1]. Then, one could vary the set of parameters to determine the effect each of them has on the mass and find some combination of changes that incorporate the mass shifts calculated in the relevant literature. If this process is done for many different states and transitions, some information could be extrapolated from the data regarding which model parameters to alter and by how much to achieve the desired shift for each state. This could therefore produce more accurate quenched models in the future that better approximate meson masses while significantly reducing the computation time and calculation work associated with continuum coupling effects. Furthermore, the work presented in this thesis is suited for this type of investigation because the model parameters have been taken outside of the matrices and therefore can be adjusted without needing to recalculate the matrix elements.

Whilst the methods presented in this thesis have been applied to bottomonium, they are by no means restricted to this specific context and may be generalised to other types of mesons. This could include states with different constituent quarks like charmonium, or potentially more exotic forms like hybrid mesons in which the gluons binding the constituent quarks are in an excited state. A prominent method of modelling their behaviour in this system is via a flux tube approach where, unlike conventional mesons, the flux tube carries non-zero angular momentum. Despite this, the angular momentum coefficients in (76) can be equally applied to hybrid mesons, as discussed in [17]. However, the spatial matrix element in (76) would be different, but can be taken from 36 for example, which calculates the breaking of chromoelectric flux tubes in an harmonic oscillator approximation. A complicating factor in hybrids, however, is that they are heavier than conventional mesons and are therefore not necessarily below threshold. Since the methods detailed in this thesis are predicated on below threshold energies, the generalisation

to hybrid mesons may not be as simple as appropriating the relevant spatial matrix element and instead involve further calculations to incorporate the above threshold range. This is also the reason why the $4S$ state is not included in these calculations, as it too lies above the threshold energy and therefore would require further treatment than what is considered in this thesis.

In summary, this thesis has aimed to put forth a comprehensive comparison of four different methods of solving the unquenched system, including a novel approach that accounts for mixing between discrete eigenstates, and provided a quantitative analysis of the induced mass shift due to continuum coupling across the four cases. However, the restriction of transitions studied, as well as various approximations and assumptions made has left significant room for additional research to be undertaken in this field, which could enhance the conclusions presented.

8 Appendix

8.1 A: Derivation of $V_{sd}(r)$

The spin-dependent term $V_{sd}(r)$ in the Hamiltonian can be expressed as

$$V_{sd}(r) = V_{SS}(r) + V_{LS}(r) + V_T(r) \tag{142}$$

the components of which pertain to the spin-spin, spin-orbit and tensor operators respectively. The spin-orbit term has the form

$$V_{LS}(r) = \left(\frac{4b}{r^3} - \frac{\sigma}{r}\right)\frac{\boldsymbol{L}\cdot\boldsymbol{S}}{2m_b^2} \tag{143}$$

where

$$\langle \boldsymbol{L}\cdot\boldsymbol{S}\rangle = \frac{J\left(J+1\right) - L\left(L+1\right) - S\left(S+1\right)}{2}. \tag{144}$$

The tensor part can be is given by

$$V_T(r) = \frac{4b}{m_b^2 r^3}T \tag{145}$$

where T has non vanishing diagonal matrix elements between the $L > 0$ spin-triplet states only:

$$\langle {}^3L_J|T|{}^3L_J\rangle = \begin{cases} -\dfrac{L}{6\left(2L+3\right)}, & J = L+1 \\ \dfrac{1}{6}, & J = L \\ -\dfrac{\left(L+1\right)}{6\left(2L-1\right)}, & J = L-1. \end{cases} \tag{146}$$

Since the spin-orbit and tensor force terms in $V_{sd}(r)$ only contain powers of r, computing their expectation values can also be solved using equation (111) and applying the appropriate coefficients. However, the spin-spin term

requires a slightly altered treatment due to the Gaussian smearing function associated with it:

$$V_{SS}(r) = \frac{32\pi b}{9m_b^2}\,\tilde{\delta}(r)\,\boldsymbol{S_q}\cdot\boldsymbol{S_{\bar{q}}} \tag{147}$$

where

$$\tilde{\delta}(r) = \left(\frac{\kappa}{\sqrt{\pi}}\right)^3 e^{-\kappa^2 r^2} \tag{148}$$

and

$$\boldsymbol{S_q}\cdot\boldsymbol{S_{\bar{q}}} = \frac{1}{2}S\left(S+1\right) - \frac{3}{4} \tag{149}$$

where $\kappa = 3.838\text{GeV}$ in [1]. The expectation value of V_{SS} therefore, is the expectation value of the exponential term in (148) with the appropriate coefficients applied. This is a similar calculation to that in equation (111), except the integral takes the form

$$\int_0^\infty r^p e^{-r^2\left(2\alpha^2+\kappa^2\right)}dr = \frac{(p-1)!!}{2^{p+\frac{3}{2}}\left(2\alpha^2+\kappa^2\right)^{\frac{p}{2}}}\sqrt{\frac{\pi}{\left(2\alpha^2+\kappa^2\right)}} \tag{150}$$

since q in the power of r is zero in this case and therefore p is even.

9 Bibliography

References

[1] Y. Lu, M. N. Anwar, and B.-S. Zou, "Coupled-channel effects for the bottomonium with realistic wave functions," *Physical Review D*, vol. 94, no. 3, p. 034021, 2016.

[2] J.-F. Liu and G.-J. Ding, "Bottomonium spectrum with coupled-channel effects," *The European Physical Journal C*, vol. 72, no. 4, pp. 1–15, 2012.

[3] P. D. Group, P. A. Zyla, R. M. Barnett, J. Beringer, O. Dahl, D. A. Dwyer, D. E. Groom, C. J. Lin, K. S. Lugovsky, E. Pianori, D. J. Robinson, C. G. Wohl, W. M. Yao, K. Agashe, G. Aielli, B. C. Allanach, C. Amsler, M. Antonelli, E. C. Aschenauer, D. M. Asner, H. Baer, S. Banerjee, L. Baudis, C. W. Bauer, J. J. Beatty, V. I. Belousov, S. Bethke, A. Bettini, O. Biebel, K. M. Black, E. Blucher, O. Buchmuller, V. Burkert, M. A. Bychkov, R. N. Cahn, M. Carena, A. Ceccucci, A. Cerri, D. Chakraborty, R. S. Chivukula, G. Cowan, G. D'Ambrosio, T. Damour, D. de Florian, A. de Gouvêa, T. DeGrand, P. de Jong, G. Dissertori, B. A. Dobrescu, M. D'Onofrio, M. Doser, M. Drees, H. K. Dreiner, P. Eerola, U. Egede, S. Eidelman, J. Ellis, J. Erler, V. V. Ezhela, W. Fetscher, B. D. Fields, B. Foster, A. Freitas, H. Gallagher, L. Garren, H. J. Gerber, G. Gerbier, T. Gershon, Y. Gershtein, T. Gherghetta, A. A. Godizov, M. C. Gonzalez-Garcia, M. Goodman, C. Grab, A. V. Gritsan, C. Grojean, M. Grünewald, A. Gurtu, T. Gutsche, H. E. Haber, C. Hanhart, S. Hashimoto, Y. Hayato, A. Hebecker, S. Heinemeyer, B. Heltsley, J. J. Hernández-Rey, K. Hikasa, J. Hisano, A. Höcker, J. Holder, A. Holtkamp, J. Huston, T. Hyodo, K. F. Johnson, M. Kado, M. Karliner, U. F. Katz, M. Kenzie, V. A. Khoze, S. R. Klein, E. Klempt, R. V. Kowalewski, F. Krauss,

M. Kreps, B. Krusche, Y. Kwon, O. Lahav, J. Laiho, L. P. Lellouch, J. Lesgourgues, A. R. Liddle, Z. Ligeti, C. Lippmann, T. M. Liss, L. Littenberg, C. Lourengo, S. B. Lugovsky, A. Lusiani, Y. Makida, F. Maltoni, T. Mannel, A. V. Manohar, W. J. Marciano, A. Masoni, J. Matthews, U. G. Meißner, M. Mikhasenko, D. J. Miller, D. Milstead, R. E. Mitchell, K. Mönig, P. Molaro, F. Moortgat, M. Moskovic, K. Nakamura, M. Narain, P. Nason, S. Navas, M. Neubert, P. Nevski, Y. Nir, K. A. Olive, C. Patrignani, J. A. Peacock, S. T. Petcov, V. A. Petrov, A. Pich, A. Piepke, A. Pomarol, S. Profumo, A. Quadt, K. Rabbertz, J. Rademacker, G. Raffelt, H. Ramani, M. Ramsey-Musolf, B. N. Ratcliff, P. Richardson, A. Ringwald, S. Roesler, S. Rolli, A. Romaniouk, L. J. Rosenberg, J. L. Rosner, G. Rybka, M. Ryskin, R. A. Ryutin, Y. Sakai, G. P. Salam, S. Sarkar, F. Sauli, O. Schneider, K. Scholberg, A. J. Schwartz, J. Schwiening, D. Scott, V. Sharma, S. R. Sharpe, T. Shutt, M. Silari, T. Sjöstrand, P. Skands, T. Skwarnicki, G. F. Smoot, A. Soffer, M. S. Sozzi, S. Spanier, C. Spiering, A. Stahl, S. L. Stone, Y. Sumino, T. Sumiyoshi, M. J. Syphers, F. Takahashi, M. Tanabashi, J. Tanaka, M. Taševský, K. Terashi, J. Terning, U. Thoma, R. S. Thorne, L. Tiator, M. Titov, N. P. Tkachenko, D. R. Tovey, K. Trabelsi, P. Urquijo, G. Valencia, R. Van de Water, N. Varelas, G. Venanzoni, L. Verde, M. G. Vincter, P. Vogel, W. Vogelsang, A. Vogt, V. Vorobyev, S. P. Wakely, W. Walkowiak, C. W. Walter, D. Wands, M. O. Wascko, D. H. Weinberg, E. J. Weinberg, M. White, L. R. Wiencke, S. Willocq, C. L. Woody, R. L. Workman, M. Yokoyama, R. Yoshida, G. Zanderighi, G. P. Zeller, O. V. Zenin, R. Y. Zhu, S. L. Zhu, F. Zimmermann, J. Anderson, T. Basaglia, V. S. Lugovsky, P. Schaffner, and W. Zheng, "Review of Particle Physics," *Progress of Theoretical and Experimental Physics*, vol. 2020, 08 2020. 083C01.

[4] J. Huston, K. Rabbertz, and G. Zanderighi, "update to the quantum chromodynamics review (2019)," *URL http://pdg. lbl.*

gov/2019/reviews/rpp2019-rev-qcd. pdf, 2019.

[5] G. Sterman, J. Smith, J. C. Collins, J. Whitmore, R. Brock, J. Huston, J. Pumplin, W.-K. Tung, H. Weerts, C.-P. Yuan, *et al.*, "Handbook of perturbative qcd," *Reviews of Modern Physics*, vol. 67, no. 1, p. 157, 1995.

[6] J. C. Collins, D. E. Soper, and G. Sterman, "Factorization of hard processes in qcd," in *Perturbative QCD*, pp. 1–91, World Scientific, 1989.

[7] R. Gupta, "Introduction to lattice qcd," *arXiv preprint hep-lat/9807028*, 1998.

[8] M. A. Clark, R. Babich, K. Barros, R. C. Brower, and C. Rebbi, "Solving lattice qcd systems of equations using mixed precision solvers on gpus," *Computer Physics Communications*, vol. 181, no. 9, pp. 1517–1528, 2010.

[9] B. Yoon, T. Bhattacharya, and R. Gupta, "Machine learning estimators for lattice qcd observables," *Physical Review D*, vol. 100, no. 1, p. 014504, 2019.

[10] H. G. Tecocoatzi and R. Bijker, "The unquenched quark model," *arXiv preprint arXiv:1506.05015*, 2015.

[11] O. W. Greenberg, "Spin and unitary-spin independence in a paraquark model of baryons and mesons," *Physical Review Letters*, vol. 13, no. 20, p. 598, 1964.

[12] I. J. Aitchison, F. E. Close, A. Gal, and D. J. Millener, "The scientific publications of richard henry dalitz, frs (1925–2006)," *Nuclear Physics A*, vol. 771, pp. 8–25, 2006.

[13] R. Kumar and F. Chand, "Asymptotic study to the n-dimensional radial schrödinger equation for the quark-antiquark system," *Communications in Theoretical Physics*, vol. 59, no. 5, p. 528, 2013.

[14] E. S. Swanson, "Unquenching the quark model and screened potentials," *Journal of Physics G: Nuclear and Particle Physics*, vol. 31, no. 7, p. 845, 2005.

[15] P. González, A. Valcarce, J. Vijande, and H. Garcilazo, "$b\bar{b}$ description with a screened potential," *arXiv preprint hep-ph/0409202*, 2004.

[16] T. Burns, "Angular momentum coefficients for meson strong decay and the unquenched quark model (charm 2013)," *arXiv preprint arXiv:1311.3583*, 2013.

[17] T. Burns, "Angular momentum coefficients for meson strong decay and unquenched quark models," *Physical Review D*, vol. 90, no. 3, p. 034009, 2014.

[18] N. Isgur and J. Paton, "A flux tube model for hadrons," *Physics Letters B*, vol. 124, no. 3-4, pp. 247–251, 1983.

[19] N. Isgur and J. Paton, "Flux-tube model for hadrons in qcd," *Physical Review D*, vol. 31, no. 11, p. 2910, 1985.

[20] G. K. C. Cheung, C. E. Thomas, D. J. Wilson, G. Moir, M. Peardon, and S. M. Ryan, "DK I = 0,$D\overline{K}$I = 0, 1 scattering and the $D_{s0}^{*}(2317)$ from lattice QCD," *JHEP*, vol. 02, p. 100, 2021.

[21] D. J. Griffiths and D. F. Schroeter, *Introduction to quantum mechanics*. Cambridge University Press, 2018.

[22] T. Barnes and E. Swanson, "Hadron loops: General theorems and application to charmonium," *Physical Review C*, vol. 77, no. 5, p. 055206, 2008.

[23] T. Burns, "Meson mass splittings in unquenched quark models (eef70)," *arXiv preprint arXiv:1411.2485*, 2014.

[24] G. B. Arfken and H. J. Weber, "Mathematical methods for physicists," 1999.

[25] S. Capstick and N. Isgur, "Baryons in a relativized quark model with chromodynamics," *Physical Review D*, vol. 34, no. 9, p. 2809, 1986.

[26] T. Burns, "Unpublished works in recursion relations," 2020.

[27] M. Abramowitz and I. A. Stegun, *Handbook of mathematical functions with formulas, graphs, and mathematical tables*, vol. 55. US Government printing office, 1964.

[28] E. Ackleh, T. Barnes, and E. Swanson, "On the mechanism of open-flavor strong decays," *Physical Review D*, vol. 54, no. 11, p. 6811, 1996.

[29] T. Barnes, F. Close, P. Page, and E. Swanson, "Higher quarkonia," *Physical Review D*, vol. 55, no. 7, p. 4157, 1997.

[30] B. Numerov, "Note on the numerical integration of d2x/dt2= f (xt)," *Astronomische Nachrichten*, vol. 230, p. 359, 1927.

[31] E. Hiyama, Y. Kino, and M. Kamimura, "Gaussian expansion method for few-body systems," *Progress in Particle and Nuclear Physics*, vol. 51, no. 1, pp. 223–307, 2003.

[32] Y. S. Kalashnikova, "Coupled-channel model for charmonium levels and an option for x (3872)," *Physical Review D*, vol. 72, no. 3, p. 034010, 2005.

[33] S. Godfrey and K. Moats, "Bottomonium mesons and strategies for their observation," *Physical Review D*, vol. 92, no. 5, p. 054034, 2015.

[34] Z.-Y. Zhou and Z. Xiao, "Comprehending heavy charmonia and their decays by hadron loop effects," *The European Physical Journal A*, vol. 50, no. 10, pp. 1–8, 2014.

[35] K. Nakamura, "Review of particle physics," *Journal of Physics G: Nuclear and Particle Physics*, vol. 37, no. 7 A, 2010.

[36] F. E. Close and P. R. Page, "The Production and decay of hybrid mesons by flux tube breaking," *Nucl. Phys. B*, vol. 443, pp. 233–254, 1995.